

## Structure of ${}^9\text{Be}$ from proton scattering at 180 MeV

S. Dixit,<sup>(a)</sup> W. Bertozzi, T. N. Buti,<sup>(b)</sup> J. M. Finn,<sup>(c)</sup> F. W. Hersman,<sup>(d)</sup> C. E. Hyde-Wright,<sup>(e)</sup>  
M. V. Hynes,<sup>(f)</sup> M. A. Kovash,<sup>(g)</sup> and B. E. Norum<sup>(h)</sup>

*Department of Physics and Laboratory for Nuclear Science, Massachusetts Institute of Technology, Cambridge, Massachusetts 02139*

J. J. Kelly

*Department of Physics and Astronomy, University of Maryland, College Park, Maryland 20742*

A. D. Bacher, G. T. Emery,<sup>(i)</sup> C. C. Foster, W. P. Jones, and D. W. Miller

*Department of Physics, Indiana University, Bloomington, Indiana 47405*

B. L. Berman

*Department of Physics, George Washington University, Washington, D.C. 20052*

D. J. Millener

*Brookhaven National Laboratory, Upton, New York 11973*

(Received 1 October 1990)

Cross section and analyzing power measurements for the scattering of 180 MeV protons are used to investigate the structure of  ${}^9\text{Be}$ . Data were collected for 24 states below 21 MeV of excitation. Detailed line-shape analysis was used to isolate several broad states. Most notably, the dependence of apparent peak position upon momentum transfer was used to separate the strong resonance listed as 6.76 MeV in standard compilations into two contributions identified as the  $\frac{7}{2}^-$  member of the ground-state rotational band, located at 6.38 MeV, and the  $\frac{9}{2}^+$  weak-coupling state, located at 6.76 MeV. Calculations of proton scattering were made using a density-dependent effective interaction in the local density approximation. The quadrupole contribution to elastic scattering was included in distorted wave Born approximation and found to have an important effect upon the analyzing power. For states dominated by a single multipolarity, neutron transition densities were fitted to  $(p,p')$  data and compared with the corresponding proton transition densities fitted to  $(e,e')$  data. We find that excitation of the rotational states and the  $\frac{9}{2}^+$  state are essentially isoscalar. Shell model calculations were performed in the full  $0\hbar\omega$  and  $1\hbar\omega$  model spaces. Suggested assignments for most states are made by comparisons of shell model calculations with data for both  $(p,p')$  and  $(e,e')$ . Similar calculations for analog states observed with the  ${}^9\text{Be}(p,n){}^9\text{B}$  reaction at 135 MeV support the proposed assignments. Finally, several relatively narrow states are observed between 18 and 21 MeV that are candidates for positive-parity states with  $T = \frac{3}{2}$ .

### I. INTRODUCTION

The spectrum of  ${}^9\text{Be}$  is surprisingly poorly known. We collected data for  ${}^9\text{Be}(p,p')$  at  $E_p = 180$  MeV primarily for the purpose of subtracting the  ${}^9\text{Be}$  background from  ${}^{16}\text{O}$  spectra measured with a BeO target,<sup>1</sup> and, in so doing, found that the positions and widths compiled in Ref. 2 describe the  ${}^9\text{Be}$  spectrum rather badly. For example, the  $\frac{7}{2}^-$  member of the  $K^\pi = \frac{3}{2}^-$  ground-state rotational band is listed at several positions between 6.4 and 6.76 MeV with no indication of an unresolved companion. In fact, when we fitted this region of our spectra using a single broad peak of variable position, we observed a smooth increase of its apparent position with scattering angle.<sup>3</sup> Therefore, we undertook a systematic investigation of the properties of the low-lying  ${}^9\text{Be}$  continuum. In this paper, we report line-shape parameters for several new states of  ${}^9\text{Be}$  and refine the parameters of several known states. Subsequently, electron scattering data for  ${}^9\text{Be}$  were ana-

lyzed using the lineshape parameters determined by the present experiment.<sup>4</sup>

We have performed shell-model calculations in the full  $0\hbar\omega$  and  $1\hbar\omega$  model space. The negative-parity spectrum was computed for  $1p$ -shell wave functions using the Cohen-Kurath interaction.<sup>5</sup> Full  $1\hbar\omega$  shell-model calculations were performed for the positive-parity spectrum using the Millener-Kurath interaction.<sup>6</sup> The details of this calculation are reported in Ref. 4. Having performed a consistent analysis of both the electron and proton scattering data, multipolarities are proposed for most states. Similar calculations have also been performed for the charge-exchange reaction  ${}^9\text{Be}(p,n){}^9\text{B}$  at 135 MeV and compared with existing data. The similarity between longitudinal form factors and  $(p,p')$  on one hand and between transverse form factors and  $(p,n)$  on the other hand allows several complementary aspects of nuclear structure to be investigated in a unified picture. The spectrum we have deduced for  ${}^9\text{Be}$  is compared in Fig. 1.

For transitions dominated by a single normal-parity multipole, the proton transition density was extracted from the electron scattering data and the neutron transition density from the proton scattering data. These states include the lowest  $\frac{5}{2}^-$ ,  $\frac{7}{2}^-$ , and  $\frac{9}{2}^+$  states. Finally, we also present data which suggest positive-parity  $T = \frac{3}{2}$  assignments for several states near 19 MeV of excitation.

The experiment and the detailed line-shape analysis of the spectra are described in Sec. II. The proton scattering data are compared in Sec. III with electron scattering data and with shell-model calculations. Similar calculations for  ${}^9\text{Be}(p,n){}^9\text{B}$  at  $E_p = 135$  MeV are compared with existing data in Sec. IV. Our conclusions are summarized in Sec. V.

## II. EXPERIMENT

### A. Experimental procedure

The experiment was performed at the Indiana University Cyclotron Facility using polarized protons with  $E_p = 179.90$  MeV. Scattered protons within a  $\pm 0.5^\circ$  angular acceptance were analyzed by the QDDM spectrometer and detected by a standard array consisting of a helical wire chamber and two plastic scintillators. Detailed descriptions of this equipment may be found in Refs. 7 and 8. The beam current was measured with an external

Faraday cup, believed to be accurate to about 1%, for angles  $\theta \geq 24^\circ$ . A smaller Faraday cup within the scattering chamber was used for  $\theta \leq 24^\circ$ . The relative normalization between internal and external cups was found to be  $0.93 \pm 0.03$ .

The beam polarization was measured approximately every eight hours using the low-energy  ${}^4\text{He}$  polarimeter located after the injector cyclotron.<sup>9</sup> The polarization was typically about 0.80 for spin up and 0.77 for spin down with little variation between measurements.

The scattering angle offset was determined by comparing elastic scattering measurements performed on either side of the beam. From the cross-section measurements, we found that  $\Delta\theta = 0.013^\circ \pm 0.005^\circ$  needs to be added to the spectrometer angle. The offset resulting from the analyzing power measurements turned out to be somewhat larger, namely,  $\Delta\theta = 0.09^\circ \pm 0.03^\circ$ . However, the latter measurement is vulnerable to false asymmetries due to alignment errors or to sideways polarization components. Therefore, we omit  $\Delta\theta$  from the data tables and claim knowledge of the scattering angle better than  $0.1^\circ$ .

Most of the data reported by this paper were taken with a self-supporting  ${}^9\text{Be}$  wafer with thickness 26.76 mg/cm<sup>2</sup>. However, the elastic peak was sometimes not included in the spectra because these data were originally collected to subtract the  ${}^9\text{Be}$  continuum from  ${}^{16}\text{O}$  data measured with BeO targets. Therefore, we also report elastic scattering data taken with BeO targets ranging in thickness between 22 and 35 mg/cm<sup>2</sup>. The average energy resolution was about 100 keV (FWHM). Comparable measurements were generally consistent to better than 5%.

We have found that the reproducibility of cross-section measurements is about 2% beyond statistical fluctuations. However, this fluctuation appears limited to normalizations and not to affect analyzing powers measured with fast spin flip. Therefore, we add an additional  $\pm 2\%$ , in quadrature, to the final cross-section uncertainties but do not include this effect in the individual cross sections comprising the analyzing power. We include an uncertainty of  $\pm 0.015$  in beam polarization to account for possible variations between polarimeter measurements.

### B. Data analysis

Since the detectors only spanned approximately 9 MeV of excitation energy, coverage of 22 MeV required three overlapping bites. Representative spectra illustrating various aspects of the experiment are shown in Figs. 2–4. Figure 2 shows a fitted spectrum for scattering spin-up protons  $18^\circ$  to the right that includes the elastic peak. Figure 3 shows a spectrum for  $34^\circ$  that illustrates the strength of the 6.5 MeV bump and which includes the broad peak at 11.28 MeV. Figure 4 shows a  $10^\circ$  spectrum which includes several relatively narrow peaks found above 14 MeV of excitation.

Several features of the spectra merit discussion. First, although the central region of the elastic peak is approximately Gaussian in shape, prominent exponential tails on both sides carry significant area. The only other sharp peak below 14 MeV is the  $\frac{5}{2}^-$  state at 2.429 MeV of exci-

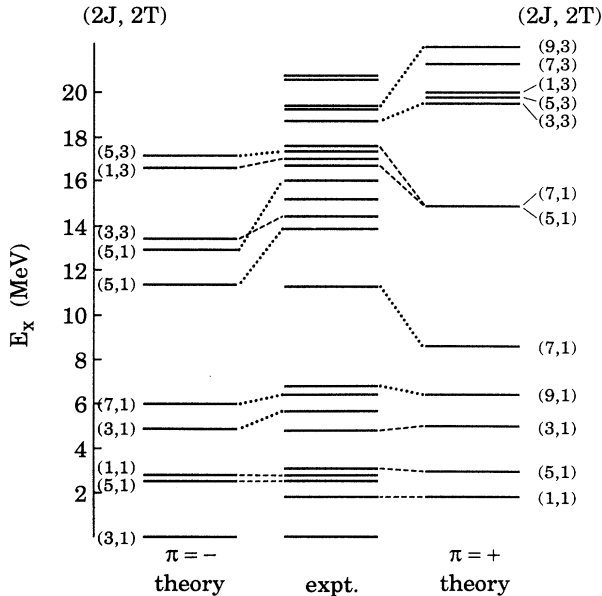


FIG. 1. Levels observed in  ${}^9\text{Be}(p,p')$  are compared with selected shell-model states. Firm correspondences between theory and experiment are indicated by dashed connecting lines, whereas tentative associations are made with dotted lines. The theoretical negative-parity spectrum was shifted down by 0.21 MeV to obtain agreement with the  $\frac{5}{2}^-$   $T = \frac{1}{2}$  state at 2.43 MeV. The theoretical positive-parity spectrum was shifted down by 1.36 MeV to obtain agreement with the  $\frac{1}{2}^+$   $T = \frac{1}{2}$  state at 1.68 MeV.

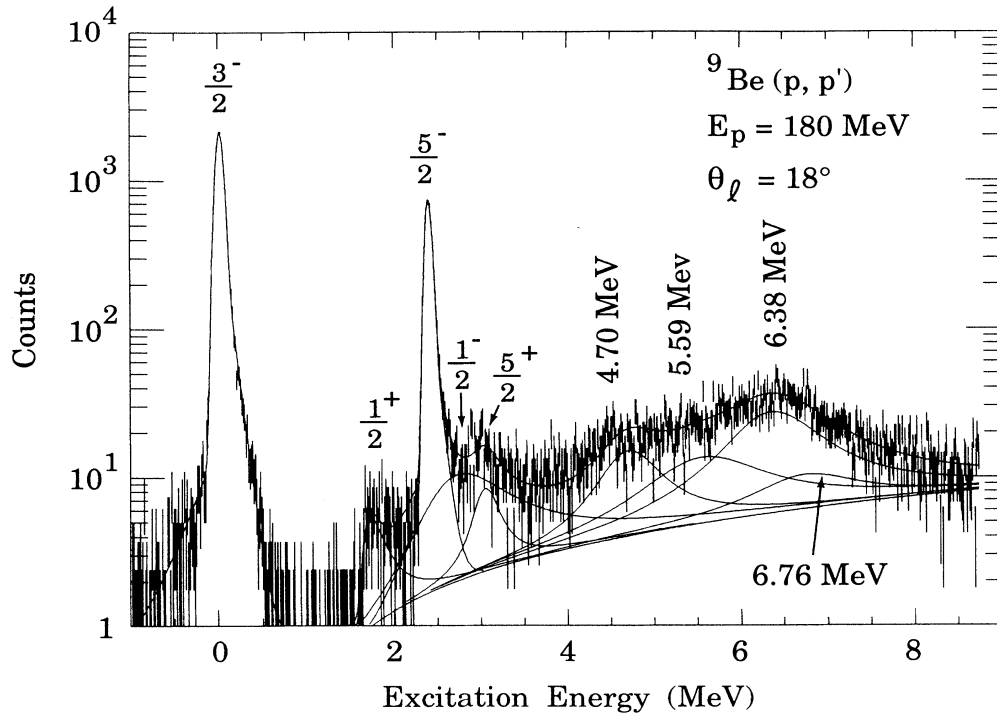


FIG. 2. Sample  ${}^9\text{Be}(p, p')$  spectrum for the scattering of 180 MeV spin-up protons  $18^\circ$  to the right in the laboratory. Note the logarithmic scale. The total fit and each individual peak are shown. At this angle the lower member of the 6.5 MeV doublet is dominant. Also note the excess strength attributed to a new peak at 5.6 MeV.

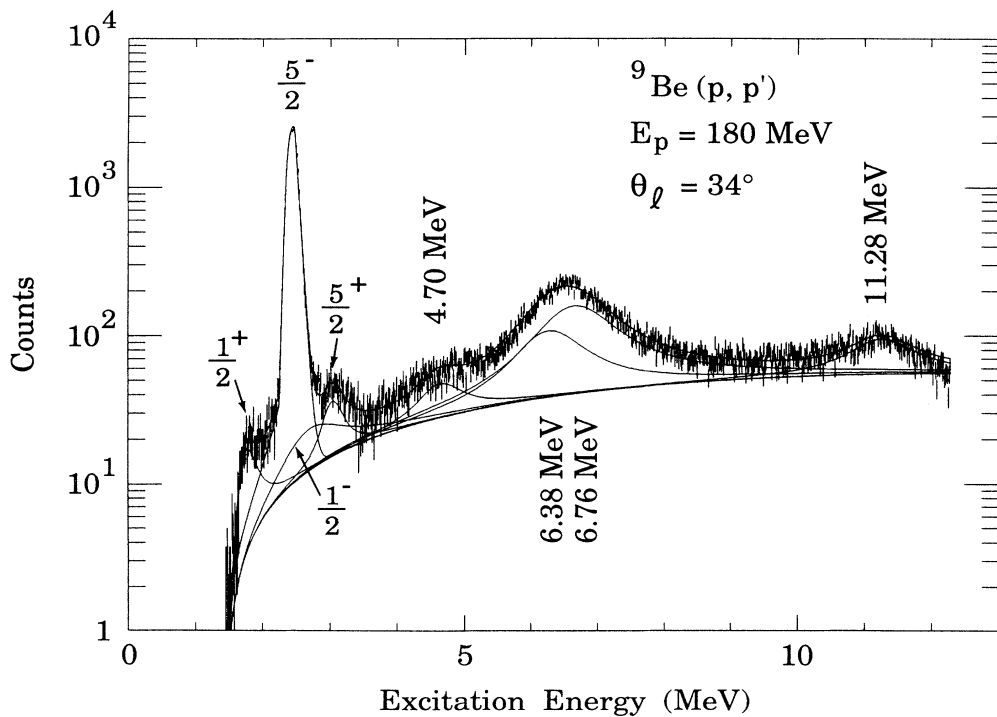


FIG. 3. Sample  ${}^9\text{Be}(p, p')$  spectrum for the scattering of 180 MeV spin-up protons  $34^\circ$  to the right in the laboratory. Note the logarithmic scale. The total fit and each individual peak are shown. At this angle the upper member of the 6.5 MeV doublet is dominant.

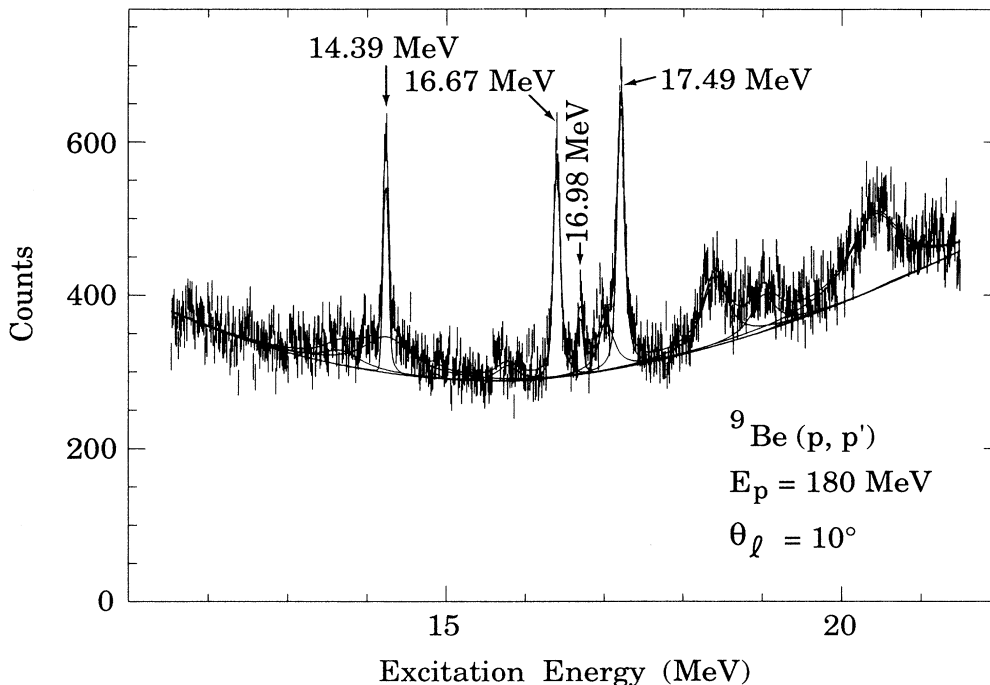


FIG. 4. Sample  ${}^9\text{Be}(p, p')$  spectrum for the scattering of 180 MeV spin-down protons  $10^\circ$  to the right in the laboratory. The four relatively narrow peaks previously studied by electron scattering (Ref. 4) are indicated. Several additional peaks above 18 MeV are evident. Note that at this momentum transfer the 19.42 MeV state is excited too weakly to be seen.

tation and is described by the same shape as the elastic peak. A substantial continuum begins at the 1.665 MeV threshold for  ${}^9\text{Be} \rightarrow {}^8\text{Be} + n$ . The  $\frac{1}{2}^+$  state at 1.68 MeV is only 15 keV above threshold, but has a width of about 217 keV. Hence, its peak shows a rather asymmetric shape. The known states at 3.05 MeV and 4.70 MeV are evident as gentle bumps in the continuum, particularly in Fig. 3.

The spectra were analyzed using the ALLFIT program and methods described in Refs. 10 and 11. Narrow peaks were fitted with the standard hypergaussian line shape, including exponential tails on either side of an asymmetric central peak. Broad peaks were described by Lorentzian intrinsic line shapes convoluted with the resolution function determined from the narrow peaks. The asymmetry of the Lorentzian line shape is particularly important for the  $\frac{1}{2}^+$  state that is located only a small fraction of its width above threshold. Convolution is important for that state and for others whose width is similar to the resolution of the experiment. The continuum was described by a polynomial background beginning at the break-up threshold. Once line-shape parameters were determined for the broad structures, an attempt was made to maintain continuity of the background across momentum bites.

The line-shape analysis was divided into several stages. The first phase was based upon the positions and widths compiled in Ref. 2. Most notably, a single Lorentzian was used to describe the broad bump listed as the  $\frac{7}{2}^-$  state at  $E_x = 6.76$  MeV with width  $\Gamma = 1.54$  MeV. A

representative spectrum illustrating the prominence of this bump is shown in Fig. 3. However, it quickly became apparent that these parameters could not provide an adequate description over the entire angular distribution. Therefore, we allowed both the position and width for a single Lorentzian to vary. The angular dependence of the fitted position is shown in Fig. 5. The apparent position of the " $\frac{7}{2}^-$ " state increases rapidly with angle, varying between about 6.2 and 6.7 MeV of excitation between momentum transfers of 0.7 and 2.0  $\text{fm}^{-1}$ . This variation encompasses the range of positions reported by the many reactions considered in the compilation. A similar analysis of electron scattering data also revealed the same behavior.<sup>4</sup> Evidently, the strong bump near 6.5 MeV actually consists of at least two broad peaks with different multiplicities. The angular distribution of the lower-energy member peaks at more forward angles than does that of the upper member.

The second step was to determine the individual positions and widths of the two members of the doublet. Having observed that the upper member is dominant at large angles, the width of the 6.76 MeV state was inferred from the single Lorentzian width for  $\theta > 32^\circ$ . The results are then  $E_x = 6.76 \pm 0.06$  MeV and  $\Gamma = 1.33 \pm 0.09$  MeV. These parameters were then held fixed throughout the subsequent analysis. A second Lorentzian with variable position and width was then inserted into the fit near  $E_x = 6.4$  MeV. The position and width of the 4.704 MeV level were held fixed to the compiled values. The forward-angle data were then used to determine the pa-

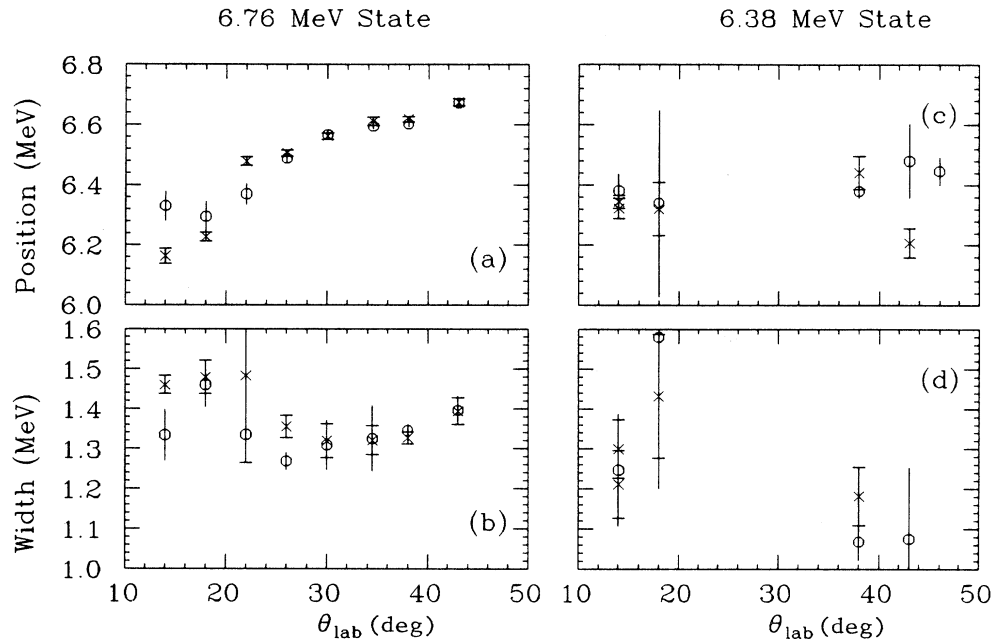


FIG. 5. Line-shape analysis of the 6.5 MeV doublet. Parameters fitted to spin-up spectra are shown as open circles and errors bars without caps, while results for spin-down are shown as crosses and error bars with caps. Panels (a) and (b) were obtained by fitting a single Lorentzian peak of variable position and width to the 6.5 MeV region of the spectra. The variation of apparent position with angle reveals the presence of an unresolved companion, whereas the stability of the width for  $\theta > 30^\circ$  was used to estimate the width of the upper member of the doublet. Panels (c) and (d) were obtained by fitting two Lorentzians to this region holding the position and width of the upper member constant.

rameters of the new state. As shown by Fig. 5, consistent values were obtained with  $E_x = 6.38 \pm 0.06$  MeV and  $\Gamma = 1.2 \pm 0.2$  MeV. These parameters were also held fixed hereafter.

The third step sought a description of the 4–6 MeV region surrounding the state listed with  $E_x = 4.704$  MeV and  $\Gamma = 0.74$  MeV. Especially at forward angles, we found it difficult to account for all of the strength in this region above a quadratic background using these parameters. A typical fit is shown in Fig. 2, wherein the excess strength between the 4.7 and 6.4 MeV suggests either a larger width for the 4.7 MeV peak or the presence of an additional peak near 5.6 MeV. The first hypothesis was tested by allowing the parameters of the 4.7 MeV peak to vary. The resultant width is then considerably larger than the tabulated 0.74 MeV, but appears to decrease with angle. Even for large angles, the apparent width  $\Gamma = 1.35$  MeV is almost twice the tabulated width.

The effect of the ambiguity in  $\Gamma(4.704)$  upon the cross sections for the 6.38 and 6.76 MeV states was determined by comparing two sets of fits. First, fits were done with  $\Gamma(4.704) = 0.74$  MeV fixed. Next, fits were done with  $\Gamma(4.704) = 1.35$  MeV. We found that the differences between the cross sections for the 6.38 and 6.76 MeV states were always less than twice the uncertainty estimated by the fitting code using fixed line-shape parameters. Therefore, the uncertainty in  $\Gamma(4.704)$  imposes no significant uncertainty upon the results for the 6.38 or 6.76 MeV states.

To describe the excess strength between 4 and 6 MeV, we decided to maintain the tabulated parameters for the 4.704 MeV peak while adding yet another Lorentzian near 5.6 MeV. The position and width were varied, keeping the parameters of surrounding peaks constant. From spectra for  $10^\circ < \theta < 22^\circ$ , we determined  $E_x = 5.59 \pm 0.1$  MeV and  $\Gamma = 1.3 \pm 0.4$  MeV.

The analysis of higher excitation regions was much simpler. When possible, Lorentzian parameters were fitted to the data. When not, tabulated parameters were used to obtain estimates of the cross sections. The resultant parameters are compared in Table I with those of the most recent compilation. The most significant difference was found for the states listed in the compilation as 11.28 and 11.81 MeV. We found no evidence for a state at 11.81 MeV. The tabulated widths yield very poor fits to our spectra. Instead the  $(p, p')$  spectra in this region can be described with a single Lorentzian at 11.28 MeV but with larger width than is attributed by Ref. 2 to either of these states. The electron scattering spectra of Glickman *et al.*<sup>4</sup> are also consistent with these conclusions. Complete details of the line-shape analysis may be found in Ref. 8.

The final step of the analysis was to determine best-fit cross sections. The line-shape parameters for all peaks listed in Table I were held fixed and only heights and backgrounds were varied during a final round of fits. The fitted areas and their estimated uncertainties were then used to determine cross sections and analyzing powers.

TABLE I. Energy levels ( $E_x$ ) and widths ( $\Gamma$ ) for states observed in  ${}^9\text{B}(p,p')$ . New values for positions or widths are marked with asterisks (\*). Widths smaller than 40 keV were neglected. Proposed assignments are given within parentheses. Unmarked parameters are taken from Ref. 2.

$E_x$ (MeV)	$\Gamma$ (MeV)	$J^\pi T$	Comments
0.		$\frac{3}{2}^- \frac{1}{2}$	
1.680(15)	0.217(10)	$\frac{1}{2}^+ \frac{1}{2}$	
2.4294(13)		$\frac{5}{2}^- \frac{1}{2}$	
2.78(12)	1.08(11)	$\frac{1}{2}^- \frac{1}{2}$	
3.049(9)	0.282(11)	$\frac{5}{2}^+ \frac{1}{2}$	
4.704(25)	0.743(55)	$\frac{3}{2}^+ \frac{1}{2}$	
5.59(10)*	1.33(36)*	$(\frac{3}{2}^- \frac{1}{2})$	
6.38(6)*	1.21(23)*	$(\frac{7}{2}^- \frac{1}{2})$	clearly member of $K = \frac{3}{2}^-$ band
6.76(6)	1.33(9)*	$(\frac{9}{2}^+ \frac{1}{2})$	assignment based on C3 angular distribution
11.28(5)*	1.10(23)*	$(\frac{7}{2}^+ \frac{1}{2})$	weak assignment based on C3 shape
13.79(3)	0.59(6)	$(\frac{5}{2}^- \frac{1}{2})$	also consistent with $J^\pi T = \frac{7}{2}^- \frac{1}{2}$
14.3926(18)		$\frac{3}{2}^- \frac{3}{2}$	
14.4(3)	$\sim 0.8$		
15.10(5)	0.35(18)*		
15.97(5)	$\sim 0.310$	$(\frac{5}{2}^- \frac{1}{2})$	also consistent with $J^\pi T = \frac{7}{2}^- \frac{1}{2}$
16.671(8)	0.041(4)	$\frac{5}{2}^+ \frac{1}{2}$	
16.976(2)		$\frac{1}{2}^- \frac{3}{2}$	
17.297(10)	$\sim 0.2$	$(\frac{5}{2}^- \frac{3}{2})$	
17.490(9)	0.047	$\frac{7}{2}^+ \frac{1}{2}$	
18.65(5)*	0.3(1)*	$(\frac{3}{2}^+ \frac{3}{2})$	assignment based on M2 shape
19.20(5)	0.31(8)		
19.42(5)*	0.6(3)*	$(\frac{9}{2}^+ \frac{3}{2})$	assignment based on M4 shape
20.53(3)*	0.6(1)*		
20.8(1)*	0.68(9)*		

The resulting angular distributions are shown in Sec. III along with theoretical calculations. As can be seen from these figures, the angular distributions are generally quite smooth and show few anomalies for the strong peaks. The cross sections for both the 6.38 and 6.76 MeV states are quite smooth, the former peaking at smaller angles than the latter. Even the data for the 4.704 and 5.6 MeV states are relatively smooth, although the 5.6 MeV state could not be followed beyond about  $q = 2.0 \text{ fm}^{-1}$ .

Tables of all these data are on deposit with PAPS.<sup>12</sup> The quoted uncertainties include only the statistical and fitting errors estimated by the fit code from the error matrix. This estimate excludes contributions from uncertainties in the line-shape parameters because these parameters were held fixed in the final analysis. Therefore, these uncertainties are somewhat underestimated, especially for weak states and for the overlapping 4.7 and 5.6 MeV states. A more complete angular distribution with considerably greater statistics would be required to improve upon these line-shape parameters.

### III. RESULTS AND INTERPRETATION

In this section, we compare the data to scattering calculations using theoretical wave functions in order to identify the most important structure components. All calculations are performed in distorted wave approximation using a density-dependent effective interaction based

upon the Paris potential.<sup>13</sup> The isoscalar spin-independent central and spin-orbit components of the interaction were replaced by the empirical effective interaction fitted to inelastic scattering data for  ${}^{16}\text{O}$  and  ${}^{28}\text{Si}$ .<sup>4</sup> The nuclear-matter interaction is applied to the finite nucleus using a local-density approximation evaluated at the site of the projectile.<sup>11</sup> Distorted waves are generated by the spherical part of the elastic optical potential, which is itself evaluated by folding the effective interaction over the ground-state density. The ground-state density was computed from the Lee and Kurath wave function,<sup>15</sup> using an oscillator parameter  $b = 1.765 \text{ fm}$  chosen to reproduce the tabulated rms charge radius.<sup>2</sup> The spin-current density is also included. The density dependence of the interaction for inelastic scattering was enhanced by the rearrangement factor derived by Cheon *et al.*<sup>16</sup> as discussed in Ref. 11.

Two shell-model calculations were performed. The negative-parity states were constructed for the full  $0\hbar\omega$   $1p$  shell using the Cohen and Kurath (6-16)  $2bme$  interaction.<sup>5</sup> A full  $1\hbar\omega$  calculation, including  $1s \rightarrow 1p$  and  $1p \rightarrow 2s1d$  contributions, was performed for the positive-parity states using the Millener and Kurath interaction.<sup>6</sup> The wave functions for most states relevant to the present investigation were presented in Ref. 4. Selected energy levels are compared with experimental levels in Fig. 1.

In constructing the transition densities, we applied effective charges of 1.6 (0.7) to isoscalar (isovector) densi-

ties and currents which carry normal-parity  $\Delta\pi = (-1)^{\Delta J}$  and which do not involve spin. These parameters are typical of normal-parity transitions in the  $p$  shell and the lower  $sd$  shell.<sup>17</sup> Unit effective charge was employed for all densities involving either abnormal parity or spin. The standard center-of-mass correction was applied to shell-model wave functions.

Similar calculations for the scattering of 135–200 MeV protons from light nuclei have been reported in Refs. 18–20. For example, it was shown that density dependence of the effective interaction is needed to obtain a good description of analyzing powers for the lowest  $\frac{3}{2}^-$  and  $\frac{5}{2}^-$  states of  ${}^9\text{Be}$  at  $E_p = 135$  MeV.<sup>18</sup> Significant improvements in elastic cross-section calculations were also obtained. Similarly, density-dependent interactions from nuclear-matter theory and transition densities fitted to  $(e, e')$  data also provide good descriptions of the data for  ${}^6\text{Li}(p, p')$  at 200 MeV.<sup>19</sup> In the latter it was also shown that distorted waves calculated using optical potentials from the folding model give better descriptions of inelastic analyzing powers for  ${}^6\text{Li}$  than do phenomenological potentials of Woods-Saxon shape.

#### A. Rotational band

The quadrupole deformation of  ${}^9\text{Be}$  is one of the largest known. Hence, the quadrupole contribution to elastic scattering is quite important. It has been shown that this contribution can be computed accurately in DWBA.<sup>20</sup> Such a calculation was reported recently for  ${}^9\text{Be}(p, p')$  at

135 MeV, wherein it was shown that the quadrupole contribution gives a good account of the elastic scattering data, particularly its unusual analyzing power, and is consistent with the rotational model for excitation of the  $\frac{5}{2}^-$  state.<sup>18</sup> Thus, we should be able to identify the  $\frac{7}{2}^-$  member of the ground-state rotational band using this approach.

Calculations based upon  $p$ -shell wave functions are compared with proton scattering data for the  $\frac{3}{2}^-$ ,  $\frac{5}{2}^-$ , and  $\frac{7}{2}^-$  members of the ground-state rotational band in Fig. 6. Contributions to elastic scattering with nonzero transfer of angular momentum are included in perturbation theory. We find that the quadrupole contribution to elastic scattering is quite important for momentum transfers beyond  $1.5 \text{ fm}^{-1}$ , but that the magnetic dipole and octupole contributions are negligible. Similarly, only the quadrupole contributions to the  $\frac{5}{2}^-$  and  $\frac{7}{2}^-$  inelastic transitions are important.

The effect of the quadrupole density upon elastic scattering is particularly strong for the analyzing power. The elastic analyzing power that results from the spherical density alone displays a much stronger oscillatory pattern beyond  $1.5 \text{ fm}^{-1}$  than does the data. Most dramatically, the spherical contribution to the analyzing power exhibits a strong positive peak at  $2.0 \text{ fm}^{-1}$  that is entirely absent from the data. The quadrupole contribution, which shares a common angular distribution with the  $\frac{5}{2}^-$  inelastic transition, is strongly negative in the same region of momentum transfer that the spherical

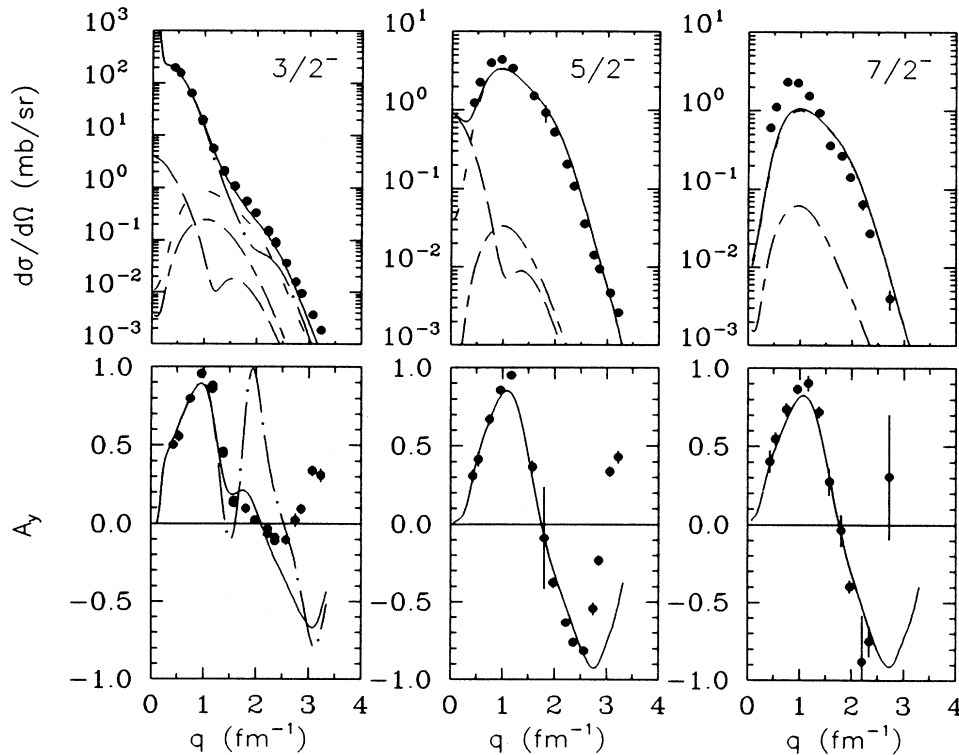


FIG. 6. Comparison between data for the  $K = \frac{3}{2}^-$  rotational band and calculations based upon shell-model wave functions. The solid curves portray complete calculations. Individual multipoles are shown as dash-dot curves for  $\Delta J = 0$ , long dashes for  $\Delta J = 1$ , short dashes for  $\Delta J = 2$ , and long-short dashed curves for  $\Delta J = 3$ .

contribution is strongly positive. Given that the two contributions to the cross section are almost equal beyond  $1.5 \text{ fm}^{-1}$ , the net result is an average analyzing power that is much smaller than either individual contribution. This effect has been shown to be important at 135 MeV (Ref. 18) and has also been observed in unpublished data for several other energies.<sup>21</sup> The discrepancies beyond  $3.0 \text{ fm}^{-1}$  may be due to defects of either the interaction or the structure or to the increasing importance of multistep processes for very large momentum transfer.

Predictions based upon the shell model for the  $\frac{5}{2}^-$  and  $\frac{7}{2}^-$  rotational states are also compared with the data in Fig. 6. The analyzing power calculations for both states agree well with the data. However, the cross-section calculations differ from the data in much the same way as did form factor calculations for electron scattering.<sup>4</sup> In particular, the calculations are low for low  $q$  and high for high  $q$  and the discrepancies are considerably worse for the  $\frac{7}{2}^-$  state. Note that analyzing powers are generally more sensitive to the identification of the multipolarity and to the details of the interaction than to the shape of the form factor. Cross-section calculations, on the other hand, reflect the shape of the form factor directly.

Given that both the proton scattering and the longitudinal form factor for electron scattering to the  $\frac{5}{2}^-$  and  $\frac{7}{2}^-$  states are dominated by a single multipole, we can ex-

tract the proton and neutron transition densities directly from these data. It is convenient to represent these densities using the Laguerre-Gaussian expansion (LGE)

$$\rho_l(r) = x^l e^{-x^2} \sum a_n L_n^{l+(1/2)}(2x^2), \quad (1)$$

where  $x = r/b$  and where  $L_n^v$  is a generalized Laguerre polynomial. The oscillator parameter  $b = 1.664 \text{ fm}^{-1}$  was chosen for  ${}^9\text{Be}$  based upon the shell model. Note that the present interpretation of the expansion parameters differ slightly from Ref. 4 in that additional form factors for center-of-mass and finite-size corrections are not applied herein. Hence, Eq. (1) describes the point-nucleon densities, whereas the analogous expansion in Ref. 4 describes shell-model densities.

The LGE coefficients for proton transition densities were fitted to the electron scattering data of Ref. 4, in effect reparametrizing those results. These densities were then used in the analysis of the proton scattering data without further adjustment. Two types of fits were then made to the proton scattering data using the methods of Refs. 22 and 23. First, we assumed that the neutron and proton transition densities were proportional and fitted a scale factor  $S$  to the data. Second, we fitted the LGE coefficients for the neutron density to the data for  $q \leq 2.7 \text{ fm}^{-1}$ , beginning with the corresponding proton parameters as initial guesses. However, upon consideration of

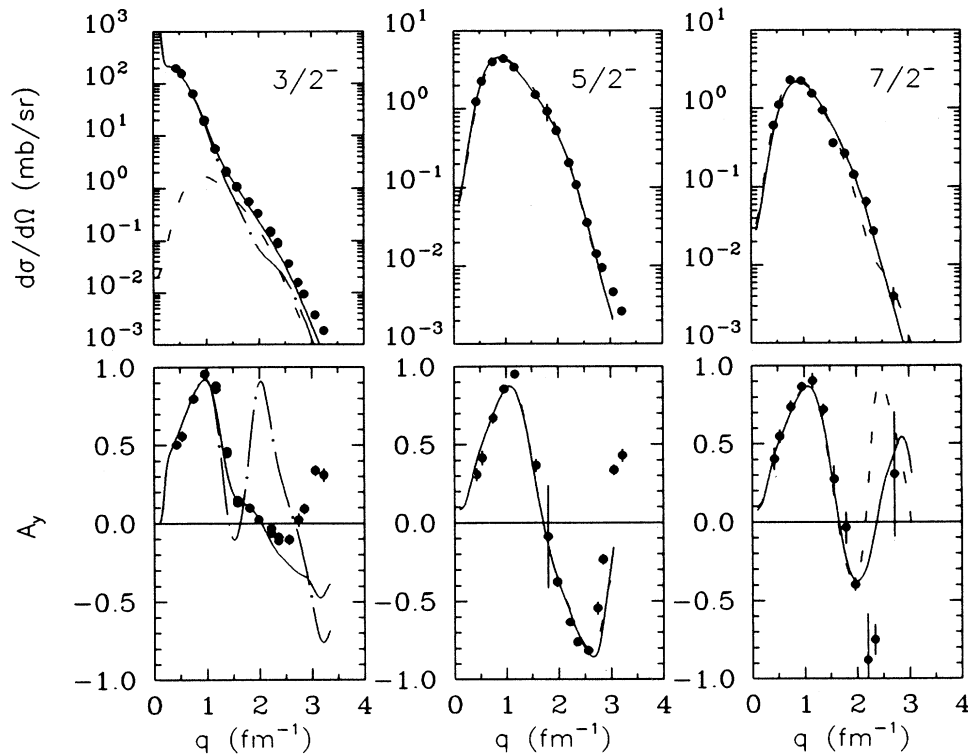


FIG. 7. Comparison between data for the  $K = \frac{3}{2}^-$  rotational band and fits based upon densities from electron scattering. For elastic scattering, solid curves portray complete calculations, the dash-dot curves show the  $\Delta J = 0$  contribution assuming that the neutron density is proportional to the proton density fitted to  $(e, e')$  and the dashed curves show the quadrupole contribution assuming  $\rho_n = \rho_p$ . For the other two states, the dashed curves show fits to the quadrupole density assuming  $\rho_n \propto \rho_p$  and the solid curves show fits to  $\rho_n$  based upon the Laguerre-Gaussian expansion.



TABLE II. Proton and neutron transition densities for  ${}^9\text{Be}$  fitted in LGE with  $b=1.664\text{ fm}^{-1}$ .

$J^\pi \Delta L$ :	$\frac{5}{2}^- \Delta L=2$		$\frac{7}{2}^- \Delta L=2$		$\frac{9}{2}^+ \Delta L=3$	
	$p$	$n$	$p$	$n$	$p$	$n$
$a_0$ ( $\text{fm}^{-3}$ )	$2.172 \times 10^{-1}$	$2.043 \times 10^{-1}$	$1.061 \times 10^{-1}$	$1.179 \times 10^{-1}$	$7.518 \times 10^{-2}$	$8.268 \times 10^{-2}$
$a_1$	$-1.262 \times 10^{-1}$	$-1.278 \times 10^{-2}$	$-2.494 \times 10^{-2}$	$-9.128 \times 10^{-3}$	$-1.632 \times 10^{-3}$	$-4.482 \times 10^{-3}$
$a_2$		$2.858 \times 10^{-3}$				$8.974 \times 10^{-4}$
$a_3$		$-2.358 \times 10^{-3}$				$3.335 \times 10^{-4}$
$M_\tau$ ( $\text{fm}^{\Delta L}$ )	5.54	6.48(30)	4.10	3.18(16)	10.19	13.0(1.4)
$R_\tau$ (fm)	3.26	3.63(15)	3.49	3.30(12)	3.60	3.64(42)

the limitations of the data for the 6.38 MeV state, it was not deemed worthwhile to estimate incompleteness errors upon the fitted densities.

The results of these two analyses are compared in Fig. 7 and the parameters are compiled in Tables II and III. For both the  $\frac{5}{2}^-$  and  $\frac{7}{2}^-$  states, we find that scaling the proton transition densities fitted to electron scattering gives descriptions of the cross section and analyzing power data for proton scattering gives descriptions of the cross section and analyzing power data for proton scattering much superior to those with shell-model densities. The scale factors for both states are close to unity, indicating transitions of predominantly isoscalar character.

We have also performed an elastic scattering calculation based upon electron scattering densities. The spherical part of the proton density was fitted to the electron scattering data using the LGE as above. We assumed that the quadrupole density has the same shape as the density fitted to the  $\frac{5}{2}^-$  state and fitted a scale factor to the electron scattering. To calculate proton scattering, we scaled the spherical part of the fitted density to  $A$  and assumed that the neutron and proton quadrupole densities are equal. We again find that the calculation based upon electron scattering is superior to the shell model. Most notably, the analyzing power calculation describes the data very well for momentum transfers less than  $2.5\text{ fm}^{-1}$ .

The neutron and proton densities fitted to the  $\frac{5}{2}^-$  and  $\frac{7}{2}^-$  states are compared in Fig. 8. We find that the two densities are virtually identical for the  $\frac{5}{2}^-$  state, but the neutron density seems to be shifted inwards relative to the proton density for the  $\frac{7}{2}^-$  state. In fact, the neutron density is closer in shape to the  $\frac{5}{2}^-$  densities than to its own proton density. Thus, only the proton density for the  $\frac{7}{2}^-$  state differs significantly from the rotational pre-

diction of a common shape. However, in the absence of electron scattering data below the peak of the form factor, it is difficult to ascribe much certainty to small shape differences. Furthermore, the fit to the analyzing power data would have been better had the proton density fitted to the  $(e, e')$  data been closer in shape to the  $\frac{5}{2}^-$  densities. Improvement of the electron scattering data for small momentum transfer would be helpful.

The isoscalar moment

$$M_0 = M_n + M_p, \quad (2)$$

where

$$M_\tau = \int dr r^{J+2} \rho_\tau(r) \quad (3)$$

for  $\tau$  equal to  $p$  or  $n$  provides a useful measure of the strength of a transition. The fitted densities give  $M_0 = 12.03$  and  $7.29\text{ fm}^2$  for the  $\frac{5}{2}^-$  and  $\frac{7}{2}^-$  states. The ratio 1.65 between these states is in good agreement with rotational prediction 1.80. We also observe that the shell model predicts  $M_n/M_p = 0.96$  for the  $\frac{5}{2}^-$  state and 0.75 for the  $\frac{7}{2}^-$  state, in good qualitative agreement with the present analysis of  $(e, e')$  and  $(p, p')$  data.

The results tabulated in Table II and displayed in Fig. 8 include estimates of uncertainties due to statistical and normalization errors, but do not include estimates of the uncertainties due to the proton densities or to errors in the reaction model. Among the former, the absence of low- $q$  data for the 6.38 MeV state might affect the magnitude of  $M_p$  or the shape of  $\rho_p$ , as described above. Among the latter, channel coupling could renormalize the cross-section calculations. The variation between the scale factor and the LGE analyses can be taken as a more realistic estimate of the uncertainty in the deduced matrix elements.

Comfort and Karp<sup>24</sup> have evaluated the effect of multi-

TABLE III. Comparison between fitted moments and shell-model predictions for the lowest  $\frac{5}{2}^-$ ,  $\frac{7}{2}^-$ , and  $\frac{9}{2}^+$  states of  ${}^9\text{Be}$ .

$J^\pi$	$\Delta L$	$M_0$ ( $\text{fm}^{\Delta L}$ )		$M_n/M_p$		$S$
		Fit	Theory	Fit	Theory	
$\frac{5}{2}^-$	2	12.0(3)	9.05	1.17(5)	0.955	1.03(5)
$\frac{7}{2}^-$	2	7.3(2)	4.41	0.78(3)	0.75	0.94(5)
$\frac{9}{2}^+$	3	23.2(1.4)	8.30	1.26(14)	2.13	1.04(6)

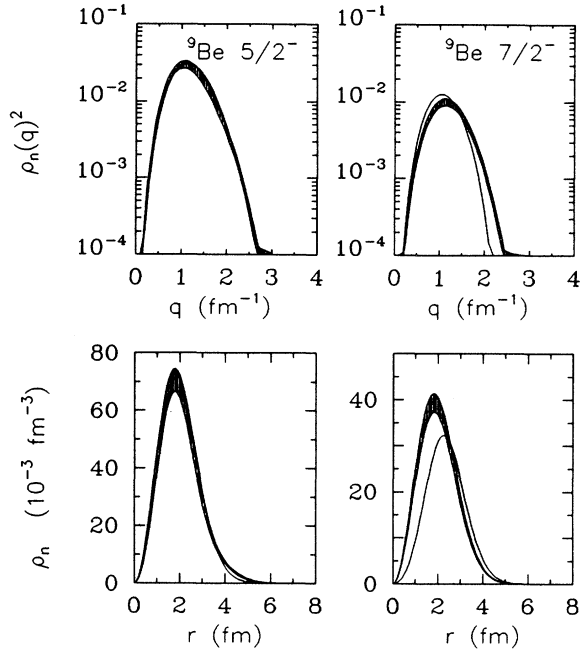


FIG. 8. Comparison between form factors and transition densities fitted to  $(e,e')$  data (solid lines) and  $(p,p')$  data (bands) for the  $\frac{5}{2}^-$  and presumed  $\frac{7}{2}^-$  members of the ground-state rotational band. The solid curves for the  $\frac{5}{2}^-$  state lie almost entirely within the bands.

step processes upon elastic scattering from  ${}^{12}\text{C}$  and for the excitation of the lowest  $2^+$  state for energies up to 185 MeV and concluded that the effects for moderate momentum transfers decrease rapidly with energy and are relatively small at 180 MeV. Roy *et al.*<sup>25</sup> have investigated the effects of channel coupling upon  ${}^9\text{Be}(p,p')$  at  $E_p = 220$  MeV, but used spherical potentials of Woods-Saxon form fitted to elastic scattering. However, the resulting potentials are unrealistic in part because the elastic quadrupole potential is important and cannot be neglected and in part because optical potentials for light nuclei deviate strongly from Woods-Saxon shape in this energy regime.

A more serious evaluation of the effect of channel coupling for  ${}^9\text{Be}$  would require evaluation of coupling potentials in the folding model using realistic interactions and good wave functions. An ambitious calculation of this type is beyond the scope of the present work, which seeks more qualitative spectroscopic information upon a large variety of transitions within a consistent framework.

The success of the present calculations, and those of Ref. 19 for  ${}^6\text{Li}(p,p')$  at 200 MeV, is an indication that single-scattering calculations based upon density-dependent effective interactions are reasonable for light nuclei in this energy regime. In particular, had channel coupling been crucial, we might have expected much greater discrepancies between the analyzing power calculations and the data. Therefore, even if the uncertainties are underestimated by the present analysis, we would not expect refinements of the reaction model to substantially alter the essential conclusion that both the  $5/2^-$  state

and the state at 6.38 MeV are excited by isoscalar  $C2$  densities of similar shape. Therefore, we identify the 6.38 MeV state with the  $\frac{7}{2}^-$  member of the ground-state rotational band.

### B. $C3$ excitations

The state at 6.76 MeV is excited with a classic  $C3$  angular distribution that is represented very well by a  $p \rightarrow d$  single-particle transition. Neither the electron nor the proton scattering data for this state can be described by a  $C2$  density of customary shape. However, we note that although the present  $\frac{9}{2}^+$  shell-model wave function describes the transverse ( $M4$ ) form factor well, the calculated longitudinal form factor (squared) requires an additional factor of 10 beyond the usual effective charge but has essentially the correct shape.<sup>4</sup> Similarly, although the shell-model calculation shown in Fig. 9 reproduces the analyzing power very well, the calculated cross section requires an enhancement factor of about 4.5. However, because the transverse form factor was predicted without the large enhancement factor, the  $M4$  contribution to proton scattering probably should not be enhanced either. If we attribute the shortfall to the matter density, the  $M4$  contribution can be neglected and proton scattering is dominated by a unique transition density. Hence, the data were analyzed by the methods

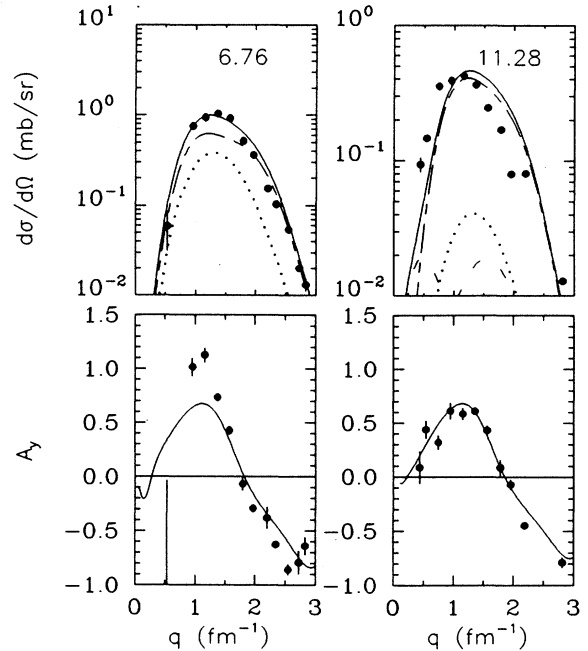


FIG. 9. Data for the states at 6.76 and 11.28 MeV are compared with calculations for the lowest  $\frac{9}{2}^+$  and  $\frac{7}{2}^+$  shell model states, respectively. Cross section calculations for the  $\frac{9}{2}^+$  and  $\frac{7}{2}^+$  states were multiplied by factors of 4.5 and 2.0, which can be compared with factors of 10 and 1.7 used for similar comparisons with  $(e,e')$  data. The solid curves portray complete calculations. Individual multipoles are shown as long dashes for  $\Delta J = 1$ , short dashes for  $\Delta J = 2$ , long-short dashed curves for  $\Delta J = 3$ , and dotted curves for  $\Delta J = 4$ .

of the preceding section.

Two fits to the data for the 6.76 MeV peak, assuming C3 excitation of a  $\frac{9}{2}^+$  state, are compared in Fig. 10. In both analyses, the proton transition density fitted to electron scattering data was held fixed. These densities are compared in Fig. 11 and the fitted parameters are listed in Tables II and III. We find that the proton scattering data are described very well using a neutron density virtually identical to the proton density. Therefore, contrary to the shell-model prediction of neutron dominance, we find the transition to be predominantly isoscalar.

Similar calculations have also been performed for the state at 11.28 MeV, which Glickman *et al.*<sup>4</sup> argued most likely corresponds to the lowest  $\frac{7}{2}^+$  model state. The shell-model calculation is compared with the data in Fig. 9. Whereas a scale factor of 1.7 was required to fit the squares of both the longitudinal and transverse form factors, the corresponding factor for the  $(p,p')$  cross section is closer to 2.0. However, because  $(e,e')$  data do not exist for  $q < 1.0 \text{ fm}^{-1}$ , the form factor is essentially undetermined at and below its peak. Moreover, the C3 shape fails to fit the  $(e,e')$  data for  $q > 2.2 \text{ fm}^{-1}$  also. Unfortunately, no single model state in the appropriate energy range provides a better description of the form factor

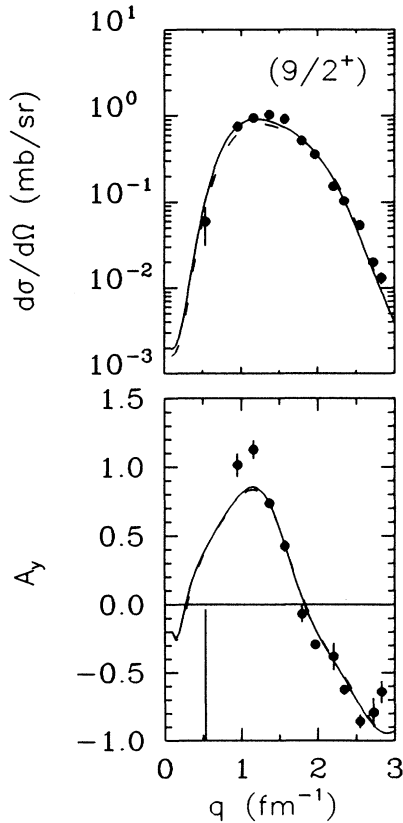


FIG. 10. Comparison between  $(p,p')$  data for the 6.76 MeV state and fits based upon C3 densities fitted to  $(e,e')$  data. The dashed curves were fitted assuming  $\rho_n \propto \rho_p$ , whereas solid curves were fitted using the Laguerre-Gaussian expansion.

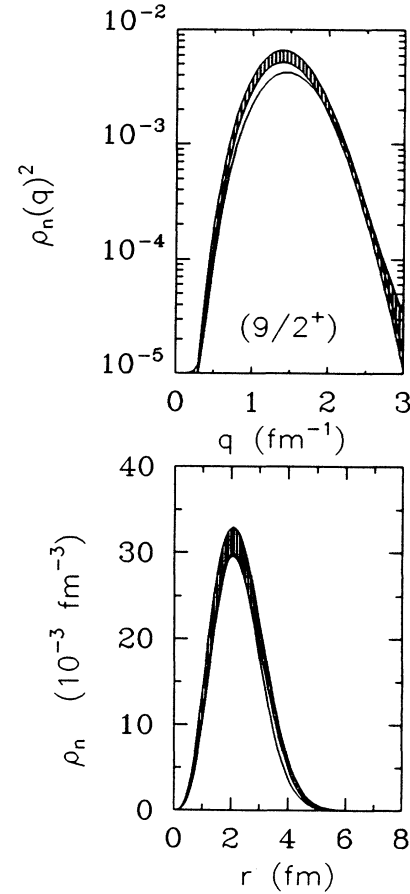


FIG. 11. Comparison between form factors and transition densities fitted to  $(e,e')$  data (solid lines) and  $(p,p')$  data (bands) for the presumed  $\frac{9}{2}^+$  state at 6.76 MeV.

data or the  $(p,p')$  data either. The fact that the low- $q$  cross section is substantially greater than expected for a C3 transition suggests that a lower multipolarity may contribute also. The characteristic normal-parity analyzing power suggest that an additional contribution, if present, is probably dominated by a C2 multipole. The most likely candidate is the second  $\frac{5}{2}^-$  state predicted to occur at about 9.8 MeV, plus a correction for the compression of the energy scale that plagues shell-model calculations for this nucleus. In the absence of a definitive identification for this state, no further analysis is warranted.

The surprising result that the state tentatively identified as  $\frac{9}{2}^+$  is reached by a nearly isoscalar transition illustrates the power of comparisons between electron and proton scattering data. From electron scattering alone, we could only conclude that the C3 strength was considerably larger than expected. Upon addition of the proton scattering data we find that a transition expected to be neutronlike is actually more nearly isoscalar in character. Although refinements of the reaction model could alter the precise value of  $M_n/M_p$ , this conclusion is not likely to change.

### C. Other low-lying states

Among the remaining states below 10 MeV, the  $\frac{1}{2}^+$  and  $\frac{5}{2}^+$  peaks are most readily resolved experimentally. Shell-model calculations for these states are compared with  $(p,p')$  data in Fig. 12. Similar calculations for  $(e,e')$  were presented in Ref. 4. The discrepancies between calculations and data for  $(p,p')$  cross sections are qualitatively similar to corresponding discrepancies in longitudinal form factors. Cross sections and form factors are considerably larger for small momentum transfer and considerably smaller for large momentum transfer than shell-model predictions. The fact that the analyzing power for the  $\frac{5}{2}^+$  state appears to lack the strong oscillation characteristic of normal-parity excitations suggests that the calculated  $\Delta J^\pi = 1^-$  and  $3^-$  amplitudes are too strong. The presence of the characteristic normal-parity analyzing power for the  $\frac{1}{2}^+$  state suggests that the  $\Delta J^\pi = 1^-$  term should dominate that transition. These observations are consistent with the findings by Glickman *et al.*<sup>4</sup> that these wave functions produce an  $M2$  form factor that is too strong and a  $C1$  form factor that is too broad for the  $\frac{1}{2}^+$  state and a  $C3$  form factor too strong for the  $\frac{5}{2}^+$  state.

Calculations for the lowest  $\frac{3}{2}^+$  shell-model state are compared in Fig. 13 with data for the state at 4.70 MeV. Although the discrepancies for the  $\frac{1}{2}^+$  and  $\frac{5}{2}^+$  states are of comparable magnitude for both  $(e,e')$  and  $(p,p')$ , and  $(p,p')$  cross section for the  $\frac{3}{2}^+$  state is more than an order

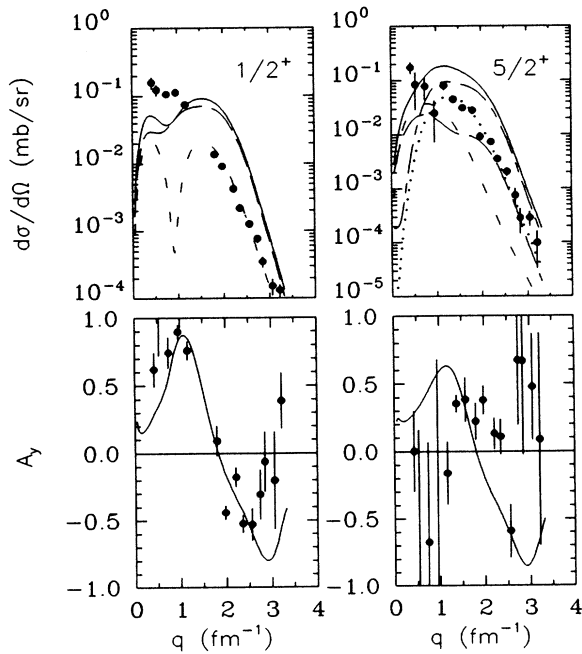


FIG. 12. Comparison between data and shell-model calculations for the lowest  $\frac{1}{2}^+$  and  $\frac{5}{2}^+$  states. The solid curves portray complete calculations. Individual multipoles are shown as long dashes for  $\Delta J=1$ , short dashes for  $\Delta J=2$ , long-short dashed curves for  $\Delta J=3$ , and dotted curves for  $\Delta J=4$ .

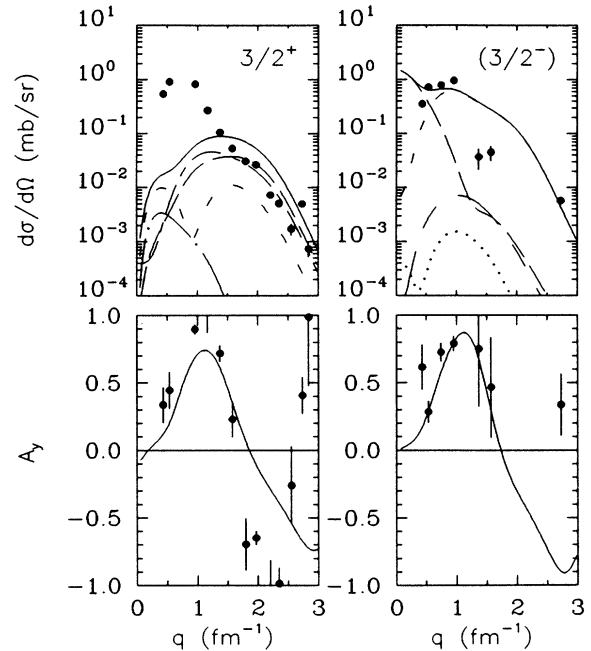


FIG. 13. Comparison between data for the peaks at 4.70 and 5.59 MeV and calculations for shell-model states with  $J^\pi = \frac{3}{2}^+$  and  $\frac{3}{2}^-$ , respectively. The solid curves portray complete calculations. Individual multipoles are shown as dash-dot curves for  $\Delta J=0$ , long dashes for  $\Delta J=1$ , short dashes for  $\Delta J=2$ , and long-short dashed curves for  $\Delta J=3$ .

of magnitude stronger than the shell-model calculation for  $q \approx 0.5 \text{ fm}^{-1}$ . Nevertheless, the analyzing power data are consistent with the prediction that normal-parity amplitudes dominate the transition. However, we found it difficult to separate the broad 4.704 MeV state from the continuum for low  $q$ . In particular, to obtain good fits to the forward angle data it seemed necessary to increase the width for the 4.704 MeV state, or to introduce additional broad structures in the same range of excitation energy, or both. Calculations for a  $\frac{3}{2}^-$  state predicted to occur at 4.88 MeV are also compared to Fig. 13 with data for the broad peak at 5.59 MeV that we used to improve the fit to forward-angle spectra. Note that the angular distributions for the 4.70 and 5.59 MeV peaks are similar to each other, but that neither assignment describes the  $(p,p')$  data for either state adequately.

Finally, we compare the data for the broad 2.78 MeV peak with calculations for the lowest  $\frac{1}{2}^-$  shell-model state in Fig. 14. The low- $q$  data are in good agreement with the predicted spin-flip strength that arises from the predominantly  $1p_{3/2} \rightarrow 1p_{1/2}$  valence neutron transition. However, the calculated cross section for higher momentum transfer could be improved by enhancing the  $C2$  contribution and reducing the  $M1$  contribution. Furthermore, the observed analyzing power displays the strong oscillatory pattern characteristic of normal-parity isoscalar excitations. Therefore, the analyzing power calculation would be improved considerably by enhancing the

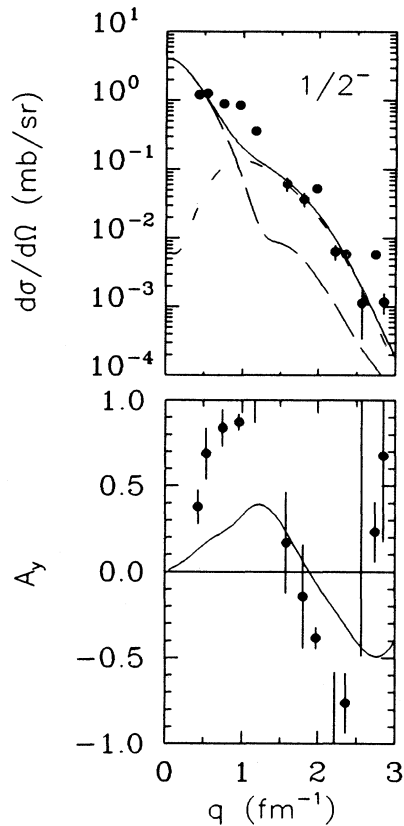


FIG. 14. Comparison between data and shell-model calculations for the lowest  $\frac{1}{2}^-$  state. The solid curves portray complete calculations. Individual multipoles are shown as long dashes for  $\Delta J=1$  and short dashes for  $\Delta J=2$ .

C2 contribution. However, this peak is rather difficult to extract because it is broad, lies on top of a continuum, and is under the much stronger  $\frac{5}{2}^-$  peak. Hence, part of the apparent enhancement of the C2 contribution may be the result of ambiguities in data analysis.

Coincidentally, even more severe difficulties with the analysis of the  ${}^9\text{Be}(p,n){}^9\text{B}$  continuum at forward angles prevent the extraction of low-lying positive-parity analog states altogether.<sup>26</sup> In that reaction, the continuum cross section is much larger than the cross sections expected for shell-model states. Therefore, the isolation of broad states from a strong continuum of undetermined shape appears problematical.

Nevertheless, the  $\frac{1}{2}^+$  and  $\frac{5}{2}^+$  states do appear to be sufficiently clear to isolate from the underlying continuum. The similarity between the  $(p,p')$  and  $(e,e')$  results suggest that oscillator wave functions in a spherical basis do not adequately describe  $1\hbar\omega$  excitations of this highly deformed nucleus.

#### D. Identification of the states at 13.79 and 15.97 MeV

The multipolarities of the states we observe at 13.79 and 15.97 MeV have not been established definitively.

On the basis of similarities observed in the  ${}^{11}\text{B}(p,{}^3\text{He}){}^9\text{Be}$  and  ${}^{11}\text{B}(p,t){}^9\text{B}$  reactions and on energy correspondences, it has been suggested that the  ${}^9\text{Be}$  states at 11.81, 13.79, and 15.97 MeV are  $J^\pi = \frac{3}{2}^-$ ,  $T = \frac{1}{2}^-$  analogs of  ${}^9\text{B}$  states at 12.06, 14.01, and 16.02 MeV.<sup>27</sup> However, the angular distributions are undistinctive and are consistent with any  $\Delta J=2$  transition from the  $\frac{3}{2}^-$  mass-11 ground state. Indeed, electron scattering calculations based upon shell-model states within several MeV of the desired energy tend to eliminate any positive-parity assignment for the 13.79 MeV state.<sup>4</sup> However, several negative-parity  $T = \frac{1}{2}^-$  states with multipolarities between  $\frac{3}{2}^-$  and  $\frac{7}{2}^-$  produce form factors with the desired shape and magnitudes within a factor of 2 of the  $(e,e')$  data for the 13.79 MeV state. Form factors for the state at 15.97 MeV have not been measured with  $(e,e')$ .

The proton scattering data for both of these states are quite similar. The cross-section angular distributions suggest  $\Delta L=2$  and the small analyzing powers suggest that abnormal-parity amplitudes are significant. Recognizing that predictions for excitation energies in this region tend to be several MeV low, proton scattering calculations have been made for several candidate transitions with energies between 10 and 16 MeV. Shell-model states with  $J^\pi = \frac{3}{2}^-$  give cross sections that are considerably larger than the forward-angle data due to the  $\Delta J^\pi = 1^+$  multipole. With appropriate normalization factors, the third and fourth  $\frac{5}{2}^-$  and second and third  $\frac{7}{2}^-$  states all give comparable fits to the present data; better data at forward angles would be needed to distinguish between these multipolarities. Higher-lying  $\frac{5}{2}^-$  and  $\frac{7}{2}^-$  states give good analyzing powers but cross sections as much as a factor of 10 too small.

Of the candidates considered, the third  $\frac{5}{2}^-$  model state agrees best with the ratio between the longitudinal and transverse form factors observed for the 13.79 MeV state; the other candidates do not describe both form factors using a single normalization factor. However, the factors for  $(e,e')$  and  $(p,p')$  are different, namely 1.0 and 0.6. Similarly, with a scale factor of 0.4, the fourth  $\frac{5}{2}^-$  shell-model state gives good agreement with the data for the state at 15.97 MeV. However, the energies of these states are calculated as 11.39 and 12.87 MeV, an average of about 2.7 MeV lower than the observed states.

Alternatively, the  $\frac{7}{2}^-$  states predicted at 10.03 and 12.22 MeV require factors 0.3 and 0.8 to reproduce the cross sections for factors observed at 13.79 and 15.97 MeV. However, the discrepancy between the energies is somewhat larger. Therefore, we choose to compare the data in Fig. 15 with calculations based upon  $\frac{5}{2}^-$  assignments for both states. Relatively good agreement between calculations and data for both cross section and analyzing power is obtained for both states.

Therefore, although the data available do not permit conclusive identification of the 13.79 and 15.97 MeV states, the preponderance of data supports assignments of either  $\frac{5}{2}^-$  or  $\frac{7}{2}^-$ . On the basis of the comparison between electron scattering and proton scattering, an assignment of  $\frac{5}{2}^-$  is preferred for the state at 13.79 MeV.

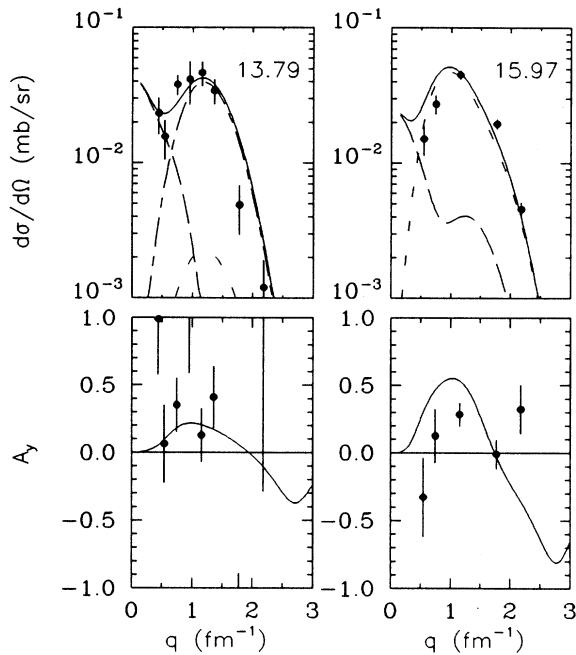


FIG. 15. Data for the states at 13.79 and 15.97 MeV are compared with shell-model calculations for third and fourth states with  $J^\pi = \frac{5}{2}^-$ , where the cross sections are renormalized by factors of 0.6 and 0.4, respectively. The solid curves portray complete calculations. Individual multipoles are shown as long dashes for  $\Delta J=1$ , short dashes for  $\Delta J=2$ , and long-short dashed curves for  $\Delta J=3$ .

### E. Negative-parity $T = \frac{3}{2}$ states

Two narrow negative-parity states with  $T = \frac{3}{2}$  have been observed in electroexcitation measurements. Calculations of the transverse form factors for the  $\frac{3}{2}^-$  state at 14.393 MeV and the  $\frac{1}{2}^-$  state at 16.976 MeV were compared in Ref. 4 with the electron scattering data of Refs. 28 and 29. With a scale factor of 1.2, that calculation for the  $\frac{3}{2}^-$  state agrees well with the  $(e, e')$  data for  $q \lesssim 1.8 \text{ fm}^{-1}$  but falls below the data for larger momentum transfer. Similarly, with a scale factor 1.4 the calculation for the  $\frac{1}{2}^-$  state agrees with the high- $q$  data for the  $E2$  form factor but falls well below the data at low  $q$  for which the  $M1$  form factor is calculated to be largest.

Similar calculations for proton scattering are compared with the data in Fig. 16 using scale factors of 1.0 and 1.4 for the 14.393 and 16.976 MeV states, respectively. Good agreement is obtained for both cross sections and analyzing powers. We note that the  $M1$  form factor for the  $\frac{1}{2}^-$  state, which is poorly described by this wave function, is not expected to contribute much to proton scattering within the measured range of momentum transfer. Hence, we obtain good agreement for  $(p, p')$  using the  $(e, e')$  scale factor.

Finally, the shell model predicts that the lowest  $\frac{5}{2}^-$  state with  $T = \frac{3}{2}$  should occur at about 17.14 MeV. In Fig. 16 we also compare calculations for that model state with the data for the state at 17.30 MeV. The strong low- $q$  cross section is well described by the calculated  $GT$  amplitude, but the calculation falls well below the cross

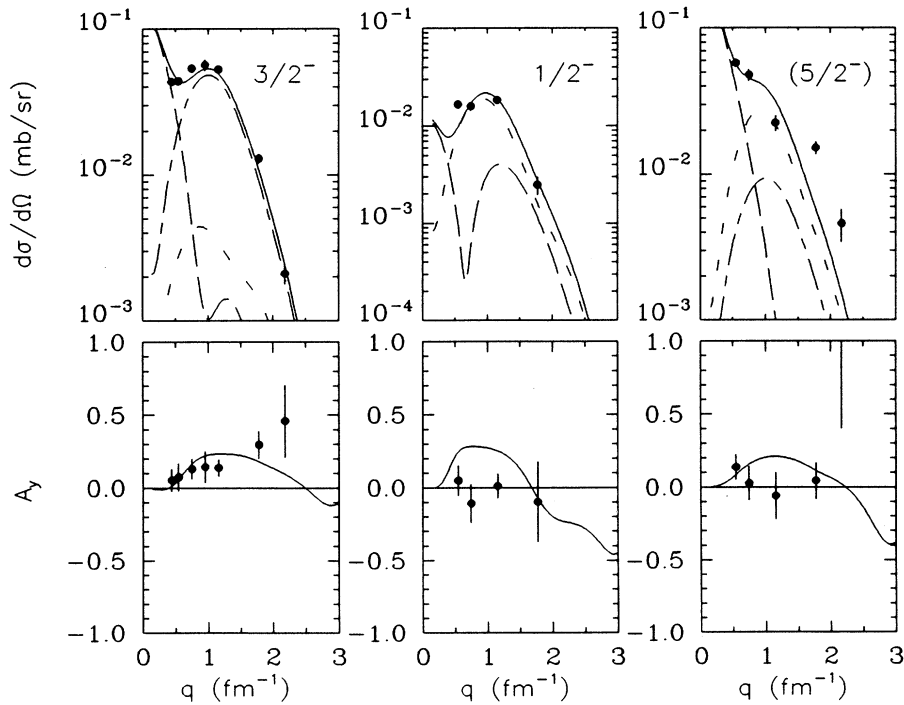


FIG. 16. Calculations for the lowest  $T = \frac{3}{2}$  shell-model states with  $J^\pi = \frac{3}{2}^-$ ,  $\frac{1}{2}^-$ , and  $\frac{5}{2}^-$ , scaled by factors of 1.0 and 1.4 and 1.0, are compared with data for the states at 14.393, 16.976, and 17.30 MeV, respectively. The solid curves portray complete calculations. Individual multipoles are shown as long dashes for  $\Delta J=1$ , short dashes for  $\Delta J=2$ , and long-short dashed curves for  $\Delta J=3$ .

section data for larger momentum transfer. If this suggested assignment is correct, perhaps another state with higher multipolarity also occurs near this excitation energy.

#### F. Narrow positive-parity states near 17 MeV

Two narrow  $T = \frac{1}{2}$  states of transverse character have been observed in electron scattering measurements at 16.671 and 17.49 MeV. Woods and Barker<sup>30</sup> suggested that these states arise by coupling  $2s1d$  valence neutron configurations with the  $2_1^+ T=1$  and  $2_2^+ T=0$  states of the  $^8\text{Be}$  core, and are narrow because of their parentage in highly excited core states. The states at 16.671 MeV was associated with a valence  $2s$  configuration because its form factor is primarily of  $M2$  character and was tentatively identified as  $\frac{5}{2}^+$ . The state at 17.49 MeV has a strong  $M4$  contribution and is thus identified with the  $[1d_{5/2} \otimes 2^+ T=1]_{\frac{7}{2}^+} T = \frac{1}{2}$  weak-coupling state.

The corresponding states in our calculation turn out to be the sixth  $\frac{5}{2}^+$  and fourth  $\frac{7}{2}^+$  states, predicted to occur at 14.85 and 14.84 MeV, respectively. Calculated transverse form factors were compared with the  $(e, e')$  data in Ref. 4. After multiplying the  $\frac{5}{2}^+$  calculation by 0.7 and the  $\frac{7}{2}^+$  calculation by 1.0, good agreement between theory and experiment is obtained for both states. Therefore, we conclude that Barker's identification of these states is correct.

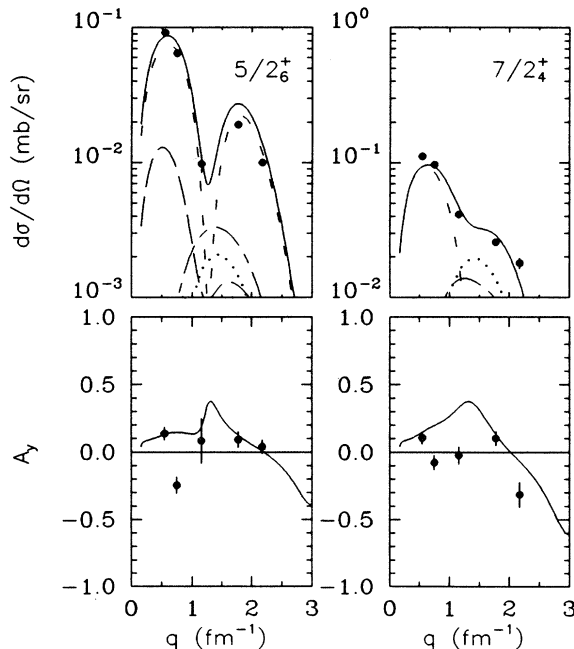


FIG. 17. Data for the  $T = \frac{1}{2}$  states at 16.67 and 17.49 MeV are compared with calculations for the sixth  $\frac{5}{2}^+$  and fourth  $\frac{7}{2}^+$  shell-model states, with both cross sections scaled by factors of 0.6. The solid curves portray complete calculations. Individual multipoles are shown as long dashes for  $\Delta J=1$ , short dashes for  $\Delta J=2$ , long-short dashed curves for  $\Delta J=3$ , and dotted curves for  $\Delta J=4$ .

Similar calculations are compared with the  $(p, p')$  data in Fig. 17, using the same scale factors of 0.6 for both states. The calculated cross sections are then in good agreement with the data for both states. The small analyzing powers confirm the abnormal-parity character of these transitions. The differences between the scale factors for the two reactions probably reflect inaccuracies for abnormal-parity components of the effective interaction that are not as well calibrated as the normal-parity components. These components of  $G$  matrices based upon the Paris and Bonn potentials differ significantly and the best choice is not yet clear.<sup>31</sup> Nevertheless, the present level of agreement lends strong support to the identification of these states.

#### G. Positive-parity $T = \frac{3}{2}$ states

We have also observed five relatively narrow states near 19 MeV. The small analyzing powers suggest abnormal parity. The forward peaking of the angular distributions for the states at 18.65, 19.2, 20.53, and 20.77 MeV suggests  $M1$  or  $M2$  assignments. The angular distribution for the state at 19.42 MeV, on the other hand, peaks at about  $1.2 \text{ fm}^{-1}$ , suggestive of an  $M4$  excitation. The most likely assignments for these states are positive-parity states with  $T = \frac{3}{2}$ , predicted to occur between 19 and 22 MeV.

Among these states, only the peaks at 18.65 and 19.42 MeV could be extracted reliably. The peaks at 20.53 and 20.77 MeV both have widths of 0.6 MeV and consequently could not be resolved. The peak at 19.2 MeV was too weak for a determination of its width. Hence, in Fig. 18 we compare shell-model calculations with data for the states at 18.65 and 19.42 MeV only.

We compare the data for the 19.42 MeV state with calculations based upon the theoretical wave function for the lowest  $\frac{9}{2}^+ T = \frac{3}{2}$  state, predicted to occur at about 22.07 MeV. Although the calculated energy is 2.6 MeV higher than this state, the absence of low- $q$  strength suggests  $\Delta L > 2$ . Within the  $1p \rightarrow 2s1d$  model space, the  $\frac{9}{2}^+$  state is reached by a nearly pure  $M4$  excitation with a particularly simple form factor. We find that excellent agreement with the data is obtained using a scale factor of 0.4. Renormalizations of this magnitude are typical of  $M4$  excitations from the  $p$  to  $sd$  shell.

The data for the 18.65 MeV state are compared with calculations for the lowest  $\frac{3}{2}^+ T = \frac{3}{2}$  state, predicted to occur at 19.50 MeV, the lowest of the  $T = \frac{3}{2}$  states with positive parity. The low- $q$  cross section is reproduced by applying a scale factor of 0.5 to the calculation. However, any  $T = \frac{3}{2}$  assignment with  $J^\pi = (\frac{1}{2} - \frac{7}{2})^+$  provides a comparable fit to this data. We prefer the  $\frac{3}{2}^+$  assignment based upon the reasonableness of the renormalization factor. Given that truncated shell-model calculations usually overestimate noncollective one-body transition strengths, renormalization factors near 0.5 fall within the range of normal expectation. The  $\frac{5}{2}^+$  and  $\frac{7}{2}^+$  states would require factors of 0.2 and 1.5, respectively, and are considered unlikely candidates.

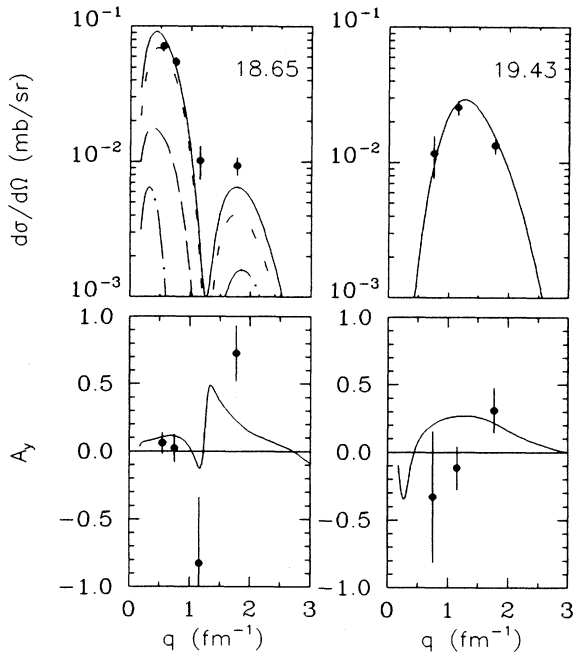


FIG. 18. Data for the states of 18.65 and 19.42 MeV are compared with shell-model calculations for the lowest  $T = \frac{3}{2}$  states with  $J^\pi = \frac{3}{2}^+$  and  $\frac{9}{2}^+$ , where the cross sections are renormalized by factors of 0.5 and 0.4, respectively. The solid curves portray complete calculations. Individual multipoles for the  $\frac{3}{2}^+$  state are shown as dash-dot curves for  $\Delta J = 0$ , long dashes for  $\Delta J = 1$ , and short dashes for  $\Delta J = 2$ . Only  $\Delta J = 4$  is significant for the  $\frac{9}{2}^+$  state.

#### IV. COMPARISON WITH ${}^9\text{Be}(p,n){}^9\text{B}$

Several of the states for which assignments have been suggested on the basis of  $(e,e')$  and  $(p,p')$  data have also been observed by Andersen-Pugh *et al.*<sup>26</sup> using the  ${}^9\text{Be}(p,n){}^9\text{B}$  reaction at 135 MeV. These states include the narrow  $\frac{3}{2}^-$  and  $\frac{5}{2}^-$  states and several broader but distinct peaks between 12 and 18 MeV excitation of  ${}^9\text{B}$ . It is of interest to compare calculations for these states with the  $(p,n)$  data shown in Figs. 19–21. Analogs of the low-lying broad states observed in  ${}^9\text{Be}$  between 1.6 and 11 MeV are too broad for reliable extraction from the continuum given the statistics achieved by the  $(p,n)$  experiment.

Calculations for the  $(p,n)$  reaction were performed using exactly the same methods as for  $(p,p')$ . The isoscalar contributions to the distorting potentials were based upon the empirical effective interaction for 135 MeV.<sup>32</sup> Different optical potentials reflecting the charge exchange and  $Q$  value were computed for the incident and exit channels. The isovector components of the interaction were obtained from the Paris-Hamburg  $G$  matrix.<sup>13</sup> Unlike  $(p,p')$ , the  $[1 + \rho(\partial/\partial\rho)]$  enhancement of inelastic density dependence was not used for charge exchange,<sup>16</sup> in part because density dependence has a much smaller effect upon  $\Delta T = 1$  components of the effective interac-

tion. The same shell-model wave functions and effective charges were employed for both reactions.

These calculations agree very well with the cross-section data for the  $\frac{3}{2}^-$  and  $\frac{5}{2}^-$  members of the  $K^\pi = \frac{3}{2}^-$  ground-state rotational band, shown in Fig. 19, and with the analyzing power data for the ground state, shown in Fig. 20. It is interesting to note that the  $(p,n)$  reaction emphasizes the  $\Delta J^\pi = 1^+$  and  $3^+$  multipoles, whereas the  $(p,p')$  reaction emphasizes the  $\Delta J^\pi = 0^+$  and  $2^+$  multipoles. Hence, the sensitivity of the  $(p,n)$  reaction for these states is most similar to the transverse electromagnetic form factor, whereas the sensitivity of  $(p,p')$  is most similar to the longitudinal form factor.

Relatively narrow states were also observed at 16.7 and 17.5 MeV which appear to be analogs of the positive-parity  $T = \frac{1}{2}$  states observed at 16.67 and 17.49 MeV in  ${}^9\text{Be}$ . The data for these states are compared with calculations for the  $5/2_6^+$  and  $7/2_4^+$  assignments which successfully described both  $(e,e')$  and  $(p,p')$  data for  ${}^9\text{Be}$ . We find that the  $(p,n)$  data are very well described using scale factors similar to those applied to the corresponding  $(e,e')$  and  $(p,p')$  calculations. Notice that the  $\Delta J^\pi = 2^-$  multipole dominates all three reactions at low momentum transfer for both states and that the  $\Delta J^\pi = 4^-$  multipole becomes important at high momentum transfer for the presumed  $\frac{7}{2}^+$  state. These characteristics support the description of the lower state as primarily  $[2s_{1/2} \otimes 2^+ T = 1]_{\frac{5}{2}^+} T = \frac{1}{2}$  and the upper state as primarily  $[1d_{5/2} \otimes 2^+ T = 1]_{\frac{7}{2}^+} T = \frac{1}{2}$ . The agreement between the scale factors for all three reactions supports the isospin structure of the model wave functions.

A relatively strong narrow peak has been observed in the delayed proton spectrum for the beta decay of  ${}^9\text{C}$  corresponding to a state in  ${}^9\text{B}$  at about 12.1 MeV. Mikolas *et al.*<sup>33</sup> argue that the assignment in best agreement with shell-model calculations of the energy and the branching ratio is  $\frac{3}{2}^- T = \frac{1}{2}$ . The similarity between beta decay and charge exchange permit this state to be observed with reasonable strength in  $(p,n)$ . In Fig. 19 we compare calculations for the third  $\frac{3}{2}^- T = \frac{1}{2}$  shell-model state with the  $(p,n)$  data for a peak at 12.2 MeV. We find that a scale factor of 0.7 yields a good fit to the data.

We have also argued that the shell-model candidate in best agreement with the  $(e,e')$  and  $(p,p')$  data for the 13.79 MeV state of  ${}^9\text{Be}$  is the third  $\frac{5}{2}^- T = \frac{1}{2}$  state and that the analog in  ${}^9\text{B}$  occurs at 14.0 MeV. A calculation is shown in Fig. 19 scaled by the same factor of 0.6 used for  $(p,p')$ . Despite the poor statistical precision of the  $(p,n)$  data, we find that this reaction is also compatible with the suggested assignment.

Finally, calculations are compared in Fig. 21 with data for the lowest  $T = \frac{3}{2}$  state, which occurs at 14.6 MeV in  ${}^9\text{B}$ . This comparison is complicated by the occurrence of two peaks with rather different widths at approximately the same excitation energy. Andersen-Pugh *et al.*<sup>26</sup> attempted to separate these peaks with a line-shape program, but uncertainty in the width of the broad peak made reliable extraction of the narrow peak of interest very difficult for small momentum transfer. Therefore, the data for both peaks are shown in Fig. 21. We find



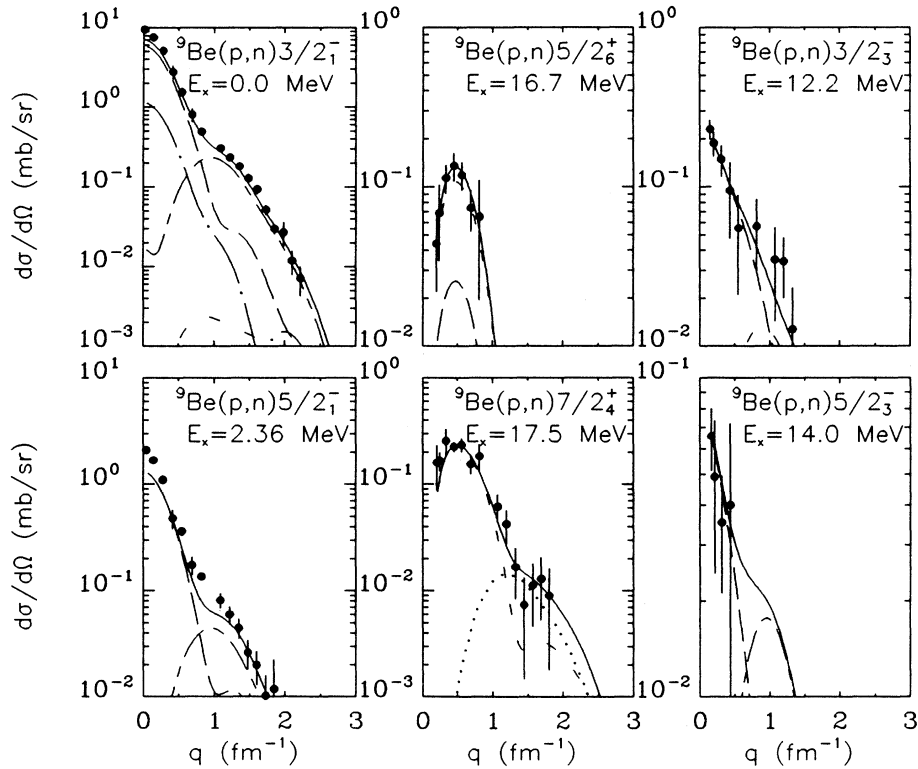


FIG. 19. Cross sections for  $T = \frac{1}{2}$  states of  ${}^9\text{Be}$  observed in the  ${}^9\text{Be}(p,n)$  reaction at 135 MeV are compared with shell-model calculations. Solid lines represent the sum of  $\Delta J = 0$  (dash-dot),  $\Delta J = 1$  (long dashes),  $\Delta J = 2$  (short dashes),  $\Delta J = 3$  (long-short), and  $\Delta J = 4$  (dots) contributions, as appropriate. Note that the cross section calculated for the 16.7 MeV peak remains below  $10^{-2}$  mb/sr for  $q > 1 \text{ fm}^{-1}$ . See text for scale factors and further details.

that the  $\Delta J^\pi = 1^+$  contribution appears to agree with the strength of the broad state, but that the strength assigned to the narrow peak is anomalously small. The  $\Delta J^\pi = 3^+$  multipole agrees well with the data for larger momentum transfer where the broad peak is less important, but could be improved upon reduction by a factor of 0.7. Given that the  $\frac{3}{2}^-$   $T = \frac{3}{2}$  state is well established and that calcu-

lations using  $p$ -shell wave functions agree relatively well with the data for  $(e, e')$  and  $(p, p')$ , we suspect that most of the low- $q$  strength observed in the vicinity of 14.6 MeV should have been assigned to this state rather than to an

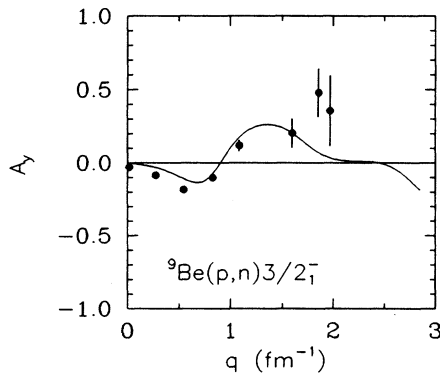


FIG. 20. Analyzing power data for the  ${}^9\text{Be}(p,n){}^9\text{B}$  ground-state transition at  $E_p = 135$  MeV is compared with a calculation based upon the Cohen-Kurath wave function.

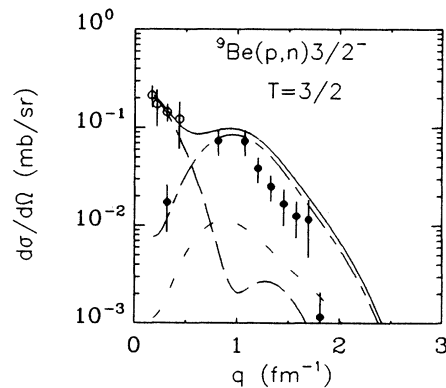


FIG. 21. Calculations for the  ${}^9\text{Be}(p,n) (3/2_1^-) T = \frac{3}{2}$  reaction at  $E_p = 135$  MeV are compared with data for the two peaks observed in  ${}^9\text{B}$  at 14.6 MeV. Data for a broad peak are shown as open circles and data for the narrow peak associated with the  $(3/2_1^-) T = \frac{3}{2}$  state are shown as closed circles. Individual multipoles are shown for  $\Delta J = 1^+$  (long dashes),  $\Delta J = 2^+$  (short dashes), and  $\Delta J = 3^+$  (long short).

TABLE IV. Scale factors deduced from comparisons between shell-model calculations and data for  $(e, e')$ ,  $(p, p')$ , and  $(p, n)$ .

$J_n^\pi T^a$	$E_x({}^9\text{Be})^b$	$E_x({}^9\text{B})^b$	$F_L^2{}^c$	$F_T^2{}^d$	$(p, p')$	$(p, n)$
$3/2_1^- 1/2$	0.0	0.0	1.0	0.7	1.0	1.0
$5/2_1^- 1/2$	2.429	2.36	1.0	1.0–1.2 <sup>e</sup>	1.0	1.0–1.5 <sup>f</sup>
$9/2_1^+ 1/2$	6.76		10.0	1.0	4.5	
$7/2_1^+ 1/2$	11.28		1.7	1.7	2.0	
$3/2_3^- 1/2$		12.2				0.7
$5/2_3^- 1/2$	13.79	14.0	1.0	1.0	0.6	0.6
$5/2_4^- 1/2$	15.97				0.4	
$5/2_6^+ 1/2$	16.67	16.7		0.7	0.6	0.7
$7/2_4^+ 1/2$	17.49	17.5		1.0	0.6	1.0
$3/2_1^- 3/2$	14.393	14.6		1.2	1.0	0.7–1.0 <sup>g</sup>
$1/2_1^- 3/2$	16.976			1.4	1.4	
$5/2_1^- 3/2$	17.30				1.0	
$3/2_1^+ 3/2$	18.65				0.5	
$9/2_1^+ 3/2$	19.42				0.4	

<sup>a</sup>Indicates association with  $n$ th shell-model state with spin  $J$ , parity  $\pi$ , and isospin  $T$ .

<sup>b</sup>Excitation energy in MeV.

<sup>c</sup>Square of the longitudinal  $(e, e')$  form factor from Ref. 4.

<sup>d</sup>Square of the transverse  $(e, e')$  form factor from Ref. 4.

<sup>e</sup> $\Delta J^\pi = 1^+$  needs to be enhanced, but  $\Delta J^\pi = 3^+$  does not.

<sup>f</sup> $\Delta J^\pi = 1^+$  needs to be enhanced, but  $\Delta J^\pi = 3^+$  does not.

<sup>g</sup>Sum of narrow and broad peaks near 14.6 MeV agrees with  $\Delta J^\pi = 1^+$  calculation, but  $\Delta J^\pi = 3^+$  calculation requires factor of 0.7.

underlying broad peak of undetermined multipolarity.

The scale factors which bring cross sections and form factors calculated with shell-model wave functions into qualitative agreement with the data for the  $(e, e')$ ,  $(p, p')$ , and  $(p, n)$  reactions are compiled in Table IV. Small differences between factors for  ${}^9\text{Be}$  and  ${}^9\text{B}$  may be attributed in part to differences between unbound single-particle wave functions for the two systems. Uncertainties in the widths of some of the states, especially for  ${}^9\text{B}$ , further complicate these comparisons. Nevertheless, the scale factors deduced for all three reactions are in good qualitative agreement for most states and support the proposed identifications. The most glaring discrepancy, as already discussed, occurs for the broad  $C3$  excitation at 6.76 MeV which requires a factor of 10 for the longitudinal form factor squared and a factor of 4.5 for the  $(p, p')$  cross section.

## V. CONCLUSIONS

Considerable insight into nuclear structure can be obtained from a consistent analysis of both electron and proton scattering data for a particular target. We have studied many states of  ${}^9\text{Be}$  using electron scattering, the scattering of 180 MeV protons, and charge exchange induced by 135 MeV protons. By comparing the data for these reactions with each other and with shell-model calculations, several new assignments and the excitations which pose the greatest challenges to theory are identified.

Although the shell model provides a reasonable description of the ground-state rotational band, the deviations between theory and experiment appear to increase

with excitation energy. A phenomenological analysis of the data shows that the transitions remain essentially isoscalar but reveals some differences between the quadrupole densities for these states. Similarly, the data for the state at 6.76 MeV are described well by a simple  $C3$  form factor but the comparison between  $(e, e')$  and  $(p, p')$  shows that this transition is mostly isoscalar, contrary to the shell-model prediction of neutron dominance.

The data for the low-lying positive-parity states are very poorly described by the  $1\hbar\omega$  shell model, with the discrepancies appearing similar for both  $(p, p')$  and  $(e, e')$ . Similarly, the broad peak associated with the lowest  $\frac{1}{2}^-$  model state appears to receive an unexpectedly strong  $C2$  contribution.

The data for several relatively narrow states above 14 MeV are described very well by the shell model. These include the lowest  $\frac{3}{2}^-$  and  $\frac{1}{2}^-$  states with  $T = \frac{3}{2}$ . The positive-parity states at 16.671 and 17.49 MeV are identified as the sixth  $\frac{5}{2}^+$  and fourth  $\frac{7}{2}^+$   $T = \frac{1}{2}$  states and owe their narrow widths to parentage in highly excited states of the core. Several narrow states above 18 MeV are assigned positive parity and  $T = \frac{3}{2}$ . Among them, the state at 19.42 MeV appears to be a pure  $M4$  excitation and hence is most likely the lowest  $\frac{9}{2}^+$   $T = \frac{3}{2}$  state.

Several other tentative assignments are suggested. In particular, the state at 13.79 MeV seems to be either  $\frac{5}{2}^-$  or  $\frac{7}{2}^-$ , with  $\frac{5}{2}^-$  preferred by both  $(p, p')$  and  $(e, e')$ . Proton scattering data for the state at 15.97 MeV are also described well by  $T = \frac{1}{2}$  shell-model states with  $J^\pi = \frac{5}{2}^-$  or  $\frac{7}{2}^-$ .

Therefore, within the  $0\hbar\omega$  and  $1\hbar\omega$  spaces, the shell model provides a good description of the structure of

most states of  ${}^9\text{Be}$  which are relatively narrow. However, the broad low-lying states have proven more difficult to describe. These difficulties may be related to deformation of the single-particle potential or to coupling to  $\alpha$ -cluster

configurations. Future theoretical investigations of deformed states in light nuclei should benefit from the availability of complementary data for the  $(e, e')$ ,  $(p, p')$ , and  $(p, n)$  reactions upon the same target.

- (a) Present address: University of Notre Dame, Notre Dame, IN 46556.
- (b) Present address: IBM Corporation, Hopewell Junction, NY 12533.
- (c) Present address: College of William & Mary, Williamsburg, VA 23185.
- (d) Present address: University of New Hampshire, Durham, NH 03824.
- (e) Present address: University of Washington, Seattle, WA 98195.
- (f) Present address: LANL, Los Alamos, NM 87545.
- (g) Present address: University of Kentucky, Lexington, KY 40506.
- (h) Present address: University of Virginia, Charlottesville, VA 22901.
- (i) Present address: Bowdoin College, Brunswick, ME 04011.
- <sup>1</sup>J. J. Kelly, J. M. Finn, W. Bertozzi, T. N. Buti, F. W. Hersman, C. Hyde-Wright, M. V. Hynes, M. A. Kovash, B. Murdock, P. Ulmer, A. D. Bacher, G. T. Emery, C. C. Foster, W. P. Jones, D. W. Miller, and B. L. Berman, *Phys. Rev. C* **41**, 2504 (1990).
- <sup>2</sup>F. Ajzenberg-Selove, *Nucl. Phys.* **A490**, 1 (1988).
- <sup>3</sup>W. Bertozzi, T. Buti, M. Finn, C. Hyde-Wright, M. A. Kovash, R. Lourie, B. Murdock, B. Pugh, P. Ulmer, A. D. Bacher, G. T. Emery, C. C. Foster, W. P. Jones, D. W. Miller, B. Norum, J. Kelly, M. V. Hynes, B. L. Berman, W. G. Love, J. A. Carr, F. Petrovich, and F. W. Hersman, IUCF Technical and Scientific report, 1982, p. 29.
- <sup>4</sup>J. P. Glickman, W. Bertozzi, T. N. Buti, S. Dixit, F. W. Hersman, C. E. Hyde-Wright, M. V. Hynes, R. W. Lourie, B. E. Norum, J. J. Kelly, B. L. Berman, and D. J. Millener, *Phys. Rev. C* **43**, 1740 (1991), the preceding paper.
- <sup>5</sup>S. Cohen and D. Kurath, *Nucl. Phys.* **73**, 1 (1965).
- <sup>6</sup>D. J. Millener and D. Kurath, *Nucl. Phys.* **A255**, 315 (1975).
- <sup>7</sup>R. D. Bent, and D. G. Madland, J. D. Cossairt, A. D. Bacher, W. P. Jones, D. W. Miller, R. E. Pollock, and P. Schwandt, IUCF Internal Report No. 73-1.
- <sup>8</sup>S. Dixit, M. S. thesis, Massachusetts Institute of Technology, 1986.
- <sup>9</sup>P. Schwandt, H. O. Meyer, W. W. Jacobs, A. D. Bacher, S. E. Vigdor, M. D. Kaitchuck, and T. R. Donoghue, *Phys. Rev. C* **26**, 55 (1982).
- <sup>10</sup>J. J. Kelly, computer code ALLFIT (unpublished).
- <sup>11</sup>J. J. Kelly, W. Bertozzi, T. N. Buti, J. M. Finn, F. W. Hersman, C. Hyde-Wright, M. V. Hynes, M. A. Kovash, B. Murdock, B. E. Norum, B. Pugh, F. N. Rad, A. D. Bacher, G. T. Emery, C. C. Foster, W. P. Jones, D. W. Miller, B. L. Berman, W. G. Love, J. A. Carr, and F. Petrovich, *Phys. Rev. C* **39**, 1222 (1989).
- <sup>12</sup>See AIP document No. PAPS PRVCA-43-1758-11 for 11 pages containing a complete tabulation of the data described in this paper. Order by PAPS number and journal reference from American Institute of Physics, Physics Auxiliary Publication Service, 335 E. 45th Street, New York, NY 10017. The price is \$1.50 for microfiche or \$5.00 for photocopies. Airmail additional. Make checks payable to the American Institute of Physics.
- <sup>13</sup>H. V. von Geramb, in *The Interaction Between Medium Energy Nucleons in Nuclei-1982*, proceedings of the Workshop, edited by H. O. Meyer, AIP Conf. Proc. No. 97 (AIP, New York, 1983), p. 44; L. Rikus, K. Nakano, and H. V. von Geramb, *Nucl. Phys.* **A414**, 413 (1984).
- <sup>14</sup>Q. Chen, J. J. Kelly, P. P. Singh, and M. C. Radhakrishna, *Phys. Rev. C* **41**, 2514 (1990).
- <sup>15</sup>T. S. H. Lee and D. Kurath, *Phys. Rev. C* **21**, 293 (1980).
- <sup>16</sup>T. Cheon, K. Takayanagi, and K. Yazaki, *Nucl. Phys.* **A437**, 301 (1985); **A445**, 227 (1985); T. Cheon and K. Takayangi, *ibid.* **A455**, 653 (1986).
- <sup>17</sup>D. J. Millener, D. I. Sober, H. Crannell, J. T. O'Brien, L. W. Fagg, S. Kowalski, C. F. Williamson, and L. Lapikas, *Phys. Rev. C* **39**, 14 (1989).
- <sup>18</sup>J. J. Kelly, *Phys. Rev. C* **38**, 1490 (1988).
- <sup>19</sup>C. W. Glover, C. C. Foster, P. Schwandt, J. R. Comfort, J. Rapaport, T. N. Taddeucci, D. Wang, G. J. Wagner, J. Seubert, A. W. Carpenter, J. A. Carr, F. Petrovich, R. J. Philpott, and M. J. Threapleton, *Phys. Rev. C* **41**, 2487 (1990).
- <sup>20</sup>A. W. Carpenter, F. Petrovich, R. J. Philpott, and J. A. Carr (unpublished); A. W. Carpenter, Ph.D. thesis, Florida State University, 1987.
- <sup>21</sup>H. Seifert, Ph.D. thesis, University of Maryland, 1990; D. Lopiano, private communication.
- <sup>22</sup>J. J. Kelly, *Phys. Rev. C* **37**, 520 (1988).
- <sup>23</sup>J. J. Kelly, Q. Chen, P. P. Singh, M. C. Radhakrishna, W. P. Jones, and H. Nann, *Phys. Rev. C* **41**, 2525 (1990).
- <sup>24</sup>J. R. Comfort and B. C. Karp, *Phys. Rev. C* **21**, 2162 (1980).
- <sup>25</sup>G. Roy, H. S. Sherif, E. D. Cooper, L. G. Greeniaus, G. A. Moss, J. Soukop, G. M. Stinson, R. Abegg, D. P. Gurd, D. A. Hutcheon, R. Liljestrang, and C. A. Miller, *Nucl. Phys.* **A442**, 686 (1985).
- <sup>26</sup>B. Andersen-Pugh, W. Bertozzi, T. N. Buti, J. M. Finn, F. W. Hersman, C. E. Hyde-Wright, J. J. Kelly, B. Murdock, M. A. Kovash, B. D. Anderson, A. R. Baldwin, A. Fazely, C. Lebo, R. Madey, J. W. Watson, C. C. Foster, J. A. Carr, and F. Petrovich (unpublished); B. Pugh, Ph.D. thesis, Massachusetts Institute of Technology, 1985.
- <sup>27</sup>J. C. Hardy, J. M. Loiseaux, J. Cerny, and G. T. Garvey, *Nucl. Phys.* **A162**, 552 (1971).
- <sup>28</sup>R. W. Lourie, W. Bertozzi, T. N. Buti, J. M. Finn, F. W. Hersman, C. Hyde, J. Kelly, M. A. Kovash, S. Kowalski, M. V. Hynes, B. E. Norum, and B. L. Berman, *Phys. Rev. C* **28**, 489 (1983).
- <sup>29</sup>J. C. Bergstrom, I. P. Auer, M. Ahmad, F. J. Kline, J. H. Hough, H. S. Caplan, and J. L. Groh, *Phys. Rev. C* **7**, 2228 (1973).
- <sup>30</sup>C. L. Woods and F. C. Barker, *Nucl. Phys.* **A427**, 73 (1984).
- <sup>31</sup>K. Nakayama and W. G. Love, *Phys. Rev. C* **38**, 51 (1988).
- <sup>32</sup>J. J. Kelly, *Phys. Rev. C* **39**, 2120 (1989).
- <sup>33</sup>D. Mikolas, B. A. Brown, W. Benenson, L. H. Harwood, E. Kashy, J. A. Nolen, Jr., B. Sherrill, J. Stevenson, J. S. Winfield, Z. Q. Xie, and R. Sherr, *Phys. Rev. C* **37**, 766 (1988).